



Insight into methanol photooxidation over mono- (Au, Cu) and bimetallic (AuCu) catalysts supported on niobium pentoxide — An operando-IR study

L. Wolski^{a,b,*,}, M. El-Roz^{b,*}, M. Daturi^b, G. Nowaczyk^c, M. Ziolek^a

^a Adam Mickiewicz University, Poznań, Faculty of Chemistry, Uniwersytetu Poznańskiego 8, 61-614 Poznań, Poland

^b Laboratoire Catalyse et Spectrochimie (LCS), ENSICAEN, Université de Caen, CNRS, 6, Boulevard du Maréchal Juin, 14050 Caen Cedex, France

^c NanoBioMedical Centre, Adam Mickiewicz University, Poznań, Wszechnicy Piastowskiej 3, 61-614 Poznań, Poland



ARTICLE INFO

Keywords:

Photocatalysis
Bimetallic nanoparticles
Methanol photooxidation
Operando-IR
Niobium pentoxide

ABSTRACT

The aim of this study was to gain deeper insight into the factors determining the activity and selectivity of mono- (Au, Cu) and bimetallic (AuCu) catalysts supported on Nb_2O_5 in methanol photooxidation. For this purpose, the prepared catalysts were characterized with the use of XRD, nitrogen sorption, ICP-OES, UV-vis, XPS, TEM and FTIR spectroscopy. Photocatalytic activity of materials was evaluated with the use of *operando*-IR system under UV and visible light irradiation. It was demonstrated that under visible light irradiation, the decoration of the niobia with bimetallic nanoparticles of gold and copper led to a synergic enhancement of the photocatalyst performance relative that of monometallic and non-doped niobia photocatalysts, tested under the same reaction conditions. It was also demonstrated that selectivity over the bimetallic gold-copper/ Nb_2O_5 catalyst was strongly affected by the nature of light source: visible light promoted a total oxidation versus a partial oxidation of methanol under UV light.

1. Introduction

Development of new highly efficient photocatalysts addressed to environmentally friendly processes, aiming at elimination of organic pollutants and/or transformation of waste into more valuable products, is still an emerging issue. One of the ways to attain this objective is to gain the fundamental knowledge on the relationship between the properties of catalysts and their activity and selectivity by studying the mechanism of the photocatalytic processes. From among gas phase photocatalytic reactions, one of the most intensively studied is oxidation of methyl alcohol [1–7]. Hitherto, many scientists have paid much attention to elucidate the methanol photooxidation pathways and to determine the influence of different parameters (e.g. concentration of methanol, irradiance, presence of oxygen in the reaction media) on the activity of TiO_2 as a model semiconductor photocatalyst [1,2,4,6,7]. However, these studies have not included more complex catalytic systems.

As known, semiconductors like TiO_2 , ZnO , Nb_2O_5 cannot be efficiently activated under visible light due to their wide band gaps (ca. 3.2 eV for TiO_2 [8], ZnO [9] and Nb_2O_5 [10]). According to literature, one of the ways to improve their activity under visible light irradiation

is to design more complex catalytic systems containing plasmonic metals (e.g. Au [11–14]) and/or other cocatalysts (e.g. Cu_2O [12,15]) that are able to absorb visible light. Recently, a very interesting report on the influence of gold nanoparticles supported on SiO_2 and WO_3 on the methanol photooxidation under visible light has been published by DePuccio and Landry [16]. They found that loading of gold on the surface of these oxides allowed a significant increase in catalytic activity. Methanol photooxidation over transition metal oxides with band gaps enabling their excitation under visible light has been also studied by El-Roz et al. [5]. The authors reported that one of the key factors affecting the activity and selectivity of supported vanadium clusters in photocatalytic processes is the size of semiconductor nanoparticles. The highest activity in methanol photooxidation was characteristic of catalysts with the smallest vanadium clusters.

To these days many authors have reported that Au-Cu systems are effective photocatalysts for photoelectrochemical water splitting [17] and photocatalytic degradation of organic dyes [18]. Bimetallic gold-copper based catalysts have been also demonstrated to show an interesting activity in the catalytic oxidation of alcohols under aerobic conditions [19–22]. This allows us to assume that bimetallic Au-Cu catalysts can be promising candidates for the application in

* Corresponding authors at: Laboratoire Catalyse et Spectrochimie (LCS), ENSICAEN, Université de Caen, CNRS, 6, Boulevard du Maréchal Juin, 14050 Caen Cedex, France.

** Corresponding authors at: Adam Mickiewicz University, Poznań, Faculty of Chemistry, Uniwersytetu Poznańskiego 8, 61-614 Poznań, Poland.

E-mail addresses: wolski.lukasz@amu.edu.pl (L. Wolski), mohamad.elroz@ensicaen.fr (M. El-Roz).

photocatalytic oxidation of methanol. However, to the best of our knowledge there is no report on photocatalytic oxidation of methyl alcohol over supported bimetallic Au-Cu catalysts. The selection of niobia used in this work as a model support for gold and copper species resulted from the unique properties of this oxide, which include both the strong metal-support interaction (SMSI) and high Brønsted acidity of niobia surface [23–25]. The SMSI effect typical of niobium-containing supports can play important role in controlling the size, shape and electronic properties of gold and copper dopants, while the high acidity of niobia surface can have significant influence on the reaction selectivity. Recently, El-Roz et al. [26] have reported that selective oxidation of methyl alcohol to dimethoxymethane (DMM) requires the presence of both: redox active sites at which methyl alcohol is oxidized to formaldehyde (FA) and Brønsted acid sites (BAS) which catalyze the condensation reaction between the as-formed formaldehyde and adsorbed methanol molecules to yield dimethoxymethane. In view of these results, one can expect that niobia which exhibits both redox and acidic (BAS) sites on its surface may be promising bifunctional photocatalyst for selective oxidation of methanol to dimethoxymethane. It is also important to stress that other widely used photocatalysts, such as bulk TiO_2 , do not exhibit Brønsted acidity, and thus formation of DMM over these metal oxides is unfavorable [26].

The aim of this study is to get a deeper insight into the mechanism of methanol photooxidation over mono (Au, Cu) and bimetallic (AuCu) catalysts supported on niobium pentoxide. For this purpose, the nanoparticles of gold and copper, were introduced onto Nb_2O_5 surface by deposition-reduction (the catalyst denoted as $Au-Nb_2O_5$ DR) and wet impregnation (the catalyst denoted as $Cu-Nb_2O_5$) methods, respectively. To study the role of Au-Cu interaction in methanol photooxidation, $Cu-Nb_2O_5$ was further modified by loading of gold using deposition-reduction method (the catalyst denoted as $AuCu-Nb_2O_5$ DR). Finally, to investigate the influence of gold deposition method on the activity of niobia-based gold catalysts, two different methods of gold loading were applied, so additionally $Au-Nb_2O_5$ AP sample was obtained (Au loaded via functionalization of niobia with (3-aminopropyl)-trimethoxysilane (APTMS)). All of these materials and the pristine support, Nb_2O_5 , were characterized in details and applied in photocatalytic oxidation of methanol under UV or visible light irradiation to better understanding the effect of the metallic active sites on the photocatalysts performance.

2. Experimental

2.1. Synthesis of catalysts

2.1.1. Synthesis of Nb_2O_5

Niobium pentoxide was synthesized using the hydrothermal procedure described by Murayama et al. [27]. In a typical synthesis route, ammonium niobate(V) oxalate hydrate (Aldrich, $C_4H_4NNbO_9 \times H_2O$, 99.99%) (9.0894 g, 30 mmol) was dissolved in 200 mL of deionized water. Following 1 h of vigorous stirring, the pellucid solution was sealed in a Teflon-lined stainless-steel autoclave and heated for 24 h at 175 °C. The solid formed during the hydrothermal treatment was then separated by filtration, washed with deionized water, dried at room temperature (r.t.) and calcined for 2 h at 500 °C. The as-prepared material was denoted as Nb_2O_5 .

2.1.2. Modification of Nb_2O_5 with metals

Copper was deposited on the surface of niobia using wet impregnation method. For this purpose, copper(II) acetate (Aldrich, $Cu(CO_2CH_3)_2$, 99.99%) was dissolved in deionized water and then mixed with the support (Nb_2O_5). Following 1 h of vigorous stirring at room temperature, the mixture was sonicated for 20 min, dried for 12 h at 60 °C and then for 24 h at 80 °C, and finally calcined for 2 h at 400 °C (temperature ramp: 2 °C/min). The as-prepared catalyst was denoted as $Cu-Nb_2O_5$.

Monometallic gold catalysts were synthesized using two different approaches: deposition-reduction method (the catalyst denoted as $Au-Nb_2O_5$ DR) and anchoring of gold species on the surface of niobia grafted with (3-aminopropyl)-trimethoxysilane (APTMS) (the catalyst denoted as $Au-Nb_2O_5$ AP). The detailed synthesis procedures used for the deposition of gold are described in Supplementary Data (SD). For the synthesis of bimetallic $AuCu-Nb_2O_5$ DR catalyst, niobia was first modified with copper by wet impregnation method, and then gold was loaded on the surface of as-prepared $Cu-Nb_2O_5$ using the deposition-reduction method.

2.2. Characterization of materials

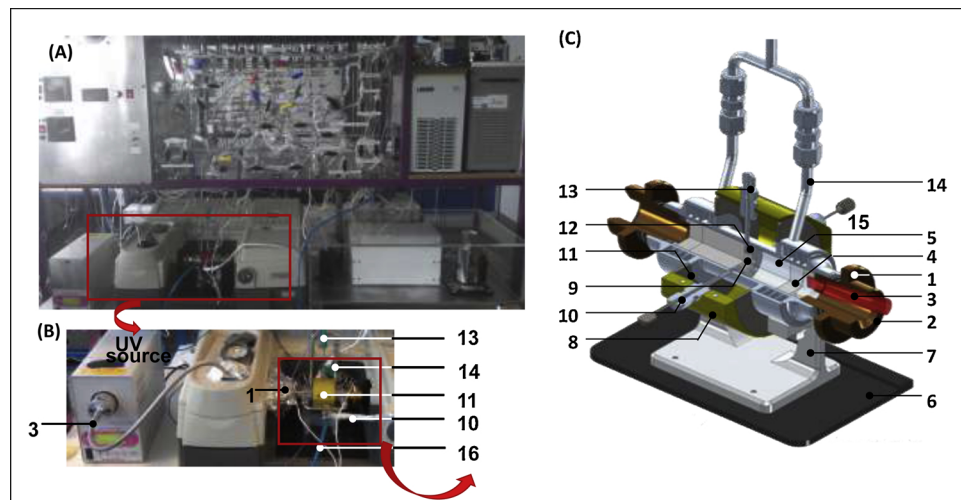
The catalysts prepared were comprehensively characterized with the use of X-ray diffraction measurements (XRD), low-temperature nitrogen adsorption-desorption, inductively coupled plasma-optical emission spectroscopy (ICP-OES), elemental analysis, transmission electron microscopy (TEM), ultraviolet-visible spectroscopy (UV-vis), X-ray photoelectron spectroscopy (XPS) and infrared spectroscopy combined with *in situ* adsorption of probe molecules (pyridine and methanol) (FTIR). The conditions of analyses with these techniques are described in Supplementary Data.

2.3. Photocatalytic tests

The photocatalysts were pressed into self-supported wafers ($\varnothing = 16$ mm, $m \approx 10.5 \text{ mg/cm}^2$) of about $65 \pm 2 \mu\text{m}$ in thickness.

The outlet gas phase evolution was followed by both IR spectroscopy and mass spectrometry. FTIR spectra of the outlet gas phase and of the surface were collected with a Nicolet 5700 FT-IR spectrometer (64 scans/spectrum) equipped with an MCT detector. The *operando* system was connected to a flow set-up [28]. Gases were introduced into the lines by mass flow controllers. The system allows the two gas mixtures, the so-called “activation” and “reaction” flows, to be prepared and sent independently to the reactor cell. The “sandwich” type reactor-cell used in this study is described in reference [3] and shown in Scheme 1. It was made of a stainless-steel cylinder that carries a toroidal sample holder in its center, where the catalyst self-supporting wafer was placed. Tightness was obtained by O-rings, and the dead volume (typically defined as the residual space between each sample face and the windows) was reduced to about 0.4 mL by filling the empty space with KBr windows placed on each side of the sample holder. The surface analysis was made possible without the superposition of the gas phase signal and fluid dynamics. Gases were introduced to the sample by 1/8-inch OD pipe and collected on the opposite side of the sample holder. In this study, the UV-vis irradiation was carried using a UV-light guide (A10014-50-0110) mounted at the entrance to the IR cell and connected to a polychromatic light of Xe-Hg lamp (for UV irradiation) (irradiance = 205 or 70 mW/cm²) or Xe lamp (for visible irradiation) (LC8 spot light Hamamatsu, L10852, 200 W; Fig. S1-SD). The lamp irradiance was measured using an ILT950 spectrilight spectroradiometer from the International Light Technologies. More details on the *operando* system for photocatalysis can be found in references [3] and [4].

The employed configuration allowed a low partial pressure of methanol to be achieved using a saturator at controlled temperature. The gas mixture composition was fixed then at 0.12 vol. % methanol and 20 vol. % O_2 in Ar and the total flow was adjusted to 20 cm³/min. The analysis of the outlet gases was performed by means of a Pfeiffer Omnistar mass spectrometer. Likewise, FT-IR spectra of the gas phase were collected using a gas microcell. The selectivity and the conversion were calculated using the calibration curves for different products of the reaction. The conversions (and the selectivity) were calculated at the steady state by taking into account the initial concentration of methanol in the gas feed (C_0), the methanol conversion, the total flow of gas mixture (and the carrier gas velocity at 25 °C) and the mass of the



catalyst (m_{cat}) (see Eq. 1).

$$\text{Conversion rate} = \frac{\text{total flow} \left[\frac{mL}{min} \right] \times \frac{C_0}{M_{MeOH} \left[\frac{g}{mol} \right]}}{\text{methanol density} \left[\frac{mg}{mL} \right] \times \frac{\text{conversion}}{m_{cat} \left[g \right]}} \quad (1)$$

All photocatalytic tests were performed step by step according to the following procedure:

- 1st step: pre-irradiation of the catalyst with high intensity UV light (polychromatic light, irradiance $\approx 205 \text{ mW/cm}^2$) (activation step),
- 2nd step: adsorption of methanol on the surface of pre-irradiated catalyst (methanol adsorption under dark conditions),
- 3rd step: irradiation of the catalyst with low intensity UV light ($\lambda = 365 \text{ nm}$; irradiance $\approx 15 \text{ mW/cm}^2$),
- 4th step: irradiation of the catalyst with high intensity UV light (polychromatic light, irradiance $\approx 205 \text{ mW/cm}^2$),
- 5th step: irradiation of the catalyst using UV light with moderate intensity (polychromatic light, irradiance $\approx 70 \text{ mW/cm}^2$),
- 6th step: irradiation of the catalyst using visible light with the wavelength higher than 390 nm (polychromatic light, irradiance $\approx 190 \text{ mW/cm}^2$).

The transition from a step to another was carried out at least two hours after reaching the steady state at each step.

3. Results and discussion

The following catalysts were used in this study: Nb_2O_5 (unmodified niobia synthesized using the hydrothermal method), $\text{Cu}-\text{Nb}_2\text{O}_5$ (the sample containing copper loaded on the surface of niobia using the wet impregnation method), $\text{Au}-\text{Nb}_2\text{O}_5$ DR (the gold catalyst prepared with the use of deposition-reduction method), $\text{Au}-\text{Nb}_2\text{O}_5$ AP (the catalyst prepared by anchoring of gold precursor on the surface of niobia grafted with APTMS), $\text{AuCu}-\text{Nb}_2\text{O}_5$ DR (the bimetallic catalyst prepared by impregnation of niobia with copper followed by deposition of gold using the deposition-reduction method).

3.1. Characterization of the catalysts

The loading of gold and copper in the catalysts was determined using ICP-OES and it is shown in Table 1. The results reveal that all the catalysts contained similar quantity of gold (ca. 2.2 wt. % of Au). For the samples containing copper, the loading of Cu was found to be of 5.4 and 5.1 wt. % for $\text{Cu}-\text{Nb}_2\text{O}_5$ and $\text{AuCu}-\text{Nb}_2\text{O}_5$ DR, respectively.

Low-temperature nitrogen sorption isotherms of the catalysts are

Scheme 1. (A) Operando setup used in this work to study the different photocatalysts. (B, C) the illustration of the operando reactor for photocatalysis: 1 - Adjusting nut for airtightness (modified for UV-guide position); 2 - IR beam; 3 - UV-light guide; 4 - Kalrez O-ring; 5 - KBr windows; 6 - Spectrometer base-plate; 7 - IR cell support; 8 - Oven location; 9 - Sample (wafer); 10 - Gas inlet; 11 - External shell; 12 - Wafer holder; 13 - Thermocouple location; 14 - Air cooling outlet; 15 - Gas outlet; 16 - Air cooling inlet.

Table 1
Characteristic of the catalysts used in this study.

Catalyst	Real metal loading ^a [wt. %]		BET surface area [m ² /g]	Number of acid sites occupied by Py after evacuation ^b [μmol/g]	
	Au	Cu		Brønsted acid sites (BAS)	Lewis acid sites (LAS)
Nb_2O_5	–	–	156	54.1	63.6
$\text{Cu}-\text{Nb}_2\text{O}_5$	–	5.4	130	–	96.6
$\text{Au}-\text{Nb}_2\text{O}_5$ DR	2.1	–	135	24.3	24.4
$\text{Au}-\text{Nb}_2\text{O}_5$ AP	2.2	–	129	27.8	39.4
$\text{AuCu}-\text{Nb}_2\text{O}_5$ DR	2.2	5.1	118	–	82.4

^a Determined by ICP-OES.

^b Calculated on the basis of Py adsorption-desorption measurements (evacuation at 150 °C for 10 min under vacuum).

shown in Fig. S2-SD. All isotherms were of type IV(a) indicating mesoporous structure of the catalysts. The presence of hysteresis loops of type H3 indicated that all materials were composed of non-rigid aggregates of plate-like particles [29]. The surface areas of the catalysts are summarized in Table 1. The largest BET surface area of 156 m²/g was characteristic of unmodified niobium pentoxide. The deposition of bulky metals proportionally reduced the surface area of niobia, and the lowest surface area of 118 m²/g was observed for $\text{AuCu}-\text{Nb}_2\text{O}_5$ DR sample containing the highest amount of modifiers.

The XRD patterns recorded for niobium pentoxide shows two distinct diffraction peaks at 2 Θ equal to 22.7 and 46.3° (Fig. 1), which are characteristic of (001) and (002) planes of layered-type structure of Nb_2O_5 , respectively [30,31]. These typical diffraction peaks of niobia are intact in the modified catalysts with gold and/or copper, indicating that the deposition of metals did not alter the structure of the support. The XRD pattern recorded for $\text{Au}-\text{Nb}_2\text{O}_5$ DR showed also four additional diffraction peaks at 2 Θ equal to 38.2, 44.4, 64.5 and 77.5°, which are characteristic of (111), (200), (220) and (311) facets of metallic gold nanoparticles, respectively [32]. In $\text{AuCu}-\text{Nb}_2\text{O}_5$ DR and $\text{Au}-\text{Nb}_2\text{O}_5$ AP samples these reflections are significantly less intense and broader, indicating smaller gold particle size for the two latter catalysts. There is no diffraction peak characteristic of metallic copper or copper/cupric oxide species detected in copper containing samples (Fig. 1). Considering relatively high copper loading (ca. 5 wt. %, Table 1), one can conclude that copper species were present in amorphous form and/or were very well dispersed on the surface of niobia.

Transmission electron microscopy gave us more information about the dispersion and the particle sizes of the metal deposited on niobium

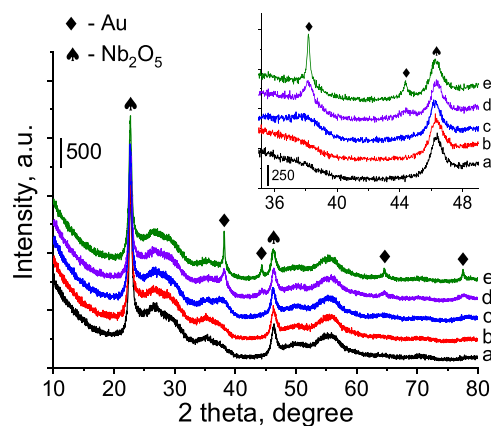


Fig. 1. XRD patterns of (a) Nb_2O_5 , (b) $\text{Cu}-\text{Nb}_2\text{O}_5$, (c) $\text{Au}-\text{Nb}_2\text{O}_5$ AP, (d) $\text{AuCu}-\text{Nb}_2\text{O}_5$ DR and (e) $\text{Au}-\text{Nb}_2\text{O}_5$ DR.

pentoxide. The modification of niobia with the metals did not affect the morphology and the structure of the support (see Fig. S3-SD). HR TEM images clearly show that there is no significant difference between crystalline structures of particular systems based on Nb_2O_5 . The interplanar spacing (marked with red lines in Fig. S3-SD) is about 0.4 nm which is in great accordance with previous HR TEM observations [33]. However, a clear difference in the Au particle size is observed on the surfaces of $\text{Au}-\text{Nb}_2\text{O}_5$ AP, $\text{AuCu}-\text{Nb}_2\text{O}_5$ DR and $\text{Au}-\text{Nb}_2\text{O}_5$ DR. Larger Au nanoparticles are detected in the last sample (see Figs. 2 and S3-SD) in agreement with the XRD data discussed above. The average sizes of gold nanoparticles were around 8.0 ± 3.3 , 4.8 ± 1.1 and 5.4 ± 2.0 nm for $\text{Au}-\text{Nb}_2\text{O}_5$ DR, $\text{Au}-\text{Nb}_2\text{O}_5$ AP and $\text{AuCu}-\text{Nb}_2\text{O}_5$ DR, respectively. The TEM-EDS mappings of Nb and Cu showed that copper species were highly dispersed on the surface of both $\text{Cu}-\text{Nb}_2\text{O}_5$ and $\text{AuCu}-\text{Nb}_2\text{O}_5$ DR (see Figs. S4 and S5-SD).

A significant decrease in the size of gold nanoparticles in the presence of copper species observed for bimetallic $\text{AuCu}-\text{Nb}_2\text{O}_5$ DR catalyst showed that some synergistic interaction between gold and copper species had to occur. The improved stability of Au-Cu bimetallic systems could result both from formation of AuCu alloys and/or formation of copper/cupric oxide species which play a role of blockade against agglomeration of gold nanoparticles making gold species more stable [33]. The second hypothesis is more probable in the case of this study. Indeed, Figs. S4 and S5-SD clearly show that there were no substantial differences in the distribution of copper species on the surface of $\text{Cu}-\text{Nb}_2\text{O}_5$ after loading of gold and all gold nanoparticles were located in close proximity to copper species. The typical inter-lattice plane of face-centered-cubic gold found by high resolution TEM (0.238 nm; Fig. S6-

SD) [34,35] on the surface of $\text{AuCu}-\text{Nb}_2\text{O}_5$ DR excluded the possible formation of AuCu alloy. Therefore, the decrease in the size of gold nanoparticles on the surface of the bimetallic samples probably resulted from structural blockade and further possible chemical interaction between gold and copper species.

Oxidation state of metals in the catalysts using X-ray photoelectron spectroscopy can reveal more information about the Au/Cu interaction in the bimetallic based samples. Analysis of Nb3d XP spectra shows that niobium in all the catalysts was present in the form of Nb^{5+} (Table 2 and Fig. S7-SD). The binding energy characteristic of $\text{Nb}^{3d_{5/2}}$ observed in this study is in agreement with the values previously reported in literature for Nb_2O_5 [36]. Deconvolution of O1s XP spectra allowed identification of four different types of oxygen species: i) lattice oxygen of $\text{CuO}/\text{Cu}_2\text{O}$ and/or strongly nucleophilic oxygen species in defected niobia (O_1) [37–43]; ii) lattice oxygen in the structure of Nb_2O_5 (O_{II}) [36,44,45]; iii) oxygen in surface hydroxyl groups (O_{III}) [36,41,45,46]; and iv) oxygen in adsorbed organic species (C–O) and/or surface siliceous species (Si–O) (O_{IV}) [41,47,48] (Table 2 and Fig. S8-SD). For $\text{Au}-\text{Nb}_2\text{O}_5$ AP, the appearance of O_{IV} is related to the presence of silica formed after decomposition of APTMS and removal of the organic part during calcination. In the catalysts containing copper (i.e. $\text{Cu}-\text{Nb}_2\text{O}_5$ and $\text{AuCu}-\text{Nb}_2\text{O}_5$ DR), the component O_{II} was reduced and it was associated with a significant increase in the content of O_1 component (Table 2). The above-mentioned increase in O_1 component content confirms successful deposition of copper species on the surface of niobia and indicates the formation of copper/cupric oxide species. The deposition of gold via DR method and/or copper led to the reduction of O_{III} component, characteristic of surface hydroxyl groups. The opposite phenomenon was observed for $\text{Au}-\text{Nb}_2\text{O}_5$ AP catalysts, in which the percentage of surface hydroxyl groups was increased (see Table 2). This increase was more likely caused by Si–OH left after APTMS decomposition (see Table S1 and Fig. S15-SD). The presence of Si–O species on silica grafted with $\text{Au}-\text{Nb}_2\text{O}_5$ AP was also confirmed by FTIR spectroscopy. Only for the samples grafted with APTMS, additional absorbance bands at ca. 3739 cm^{-1} and 3710 cm^{-1} were observed (Fig. S16-SD). The former band is characteristic of highly stable isolated silanols [49,50], while the latter could be attributed to the presence of surface silanol species interconnected by hydrogen bonding.

The Au4f XP spectra of the catalysts are shown in Fig. S9-SD. For $\text{Au}-\text{Nb}_2\text{O}_5$ AP the binding energy of spin orbital $\text{Au}4f_{7/2}$ was equal to 83.3 eV, indicating the presence of metallic gold nanoparticles with partial negative charge on their surfaces ($(\text{Au}^0)^{\delta-}$) [51]. For the monometallic gold catalyst prepared by deposition-reduction method, the majority of gold species were $(\text{Au}^0)^{\delta-}$, but a small amount of cationic gold species was also observed (Table 3). In the bimetallic AuCu catalyst, the binding energy of gold was significantly higher than that

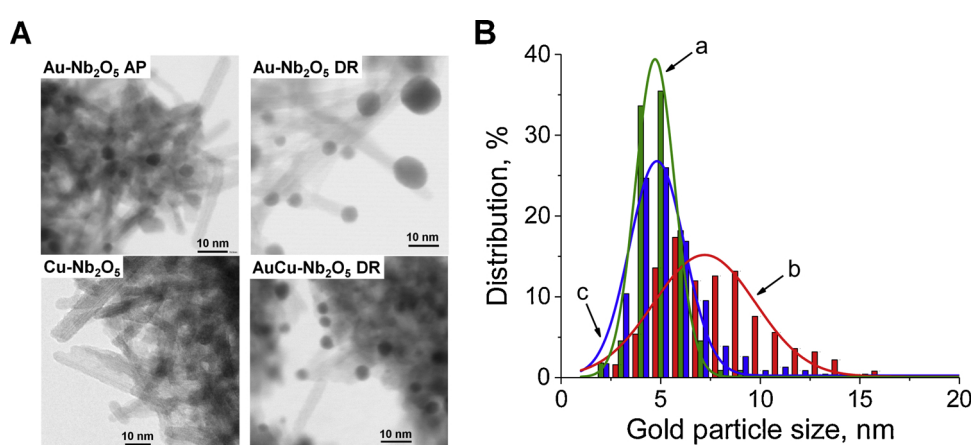


Fig. 2. (A) Representative TEM images of the catalysts and (B) gold particle size distribution in (a) $\text{Au}-\text{Nb}_2\text{O}_5$ AP, (b) $\text{Au}-\text{Nb}_2\text{O}_5$ DR and (c) $\text{AuCu}-\text{Nb}_2\text{O}_5$ DR samples basing on the TEM images.

Table 2

Surface composition of catalysts before and after methanol photooxidation studied by X-ray photoelectron spectroscopy (binding energies (BEs) normalized to BE of C1 s – 284.8 eV).

Catalyst ^a	Nb3d _{5/2}		O1s							
	Nb ⁵⁺		O _I		O _{II}		O _{III}		O _{IV}	
	BE	[%]	BE	[%]	BE	[%]	BE	[%]	BE	[%]
Nb ₂ O ₅	207.3	100.0	528.6	2.7	530.4	78.7	531.5	18.6	–	–
Nb ₂ O ₅ _r	207.2	100.0	528.3	2.6	530.3	74.4	531.5	23.0	–	–
Cu-Nb ₂ O ₅	207.2	100.0	529.6	20.1	530.5	68.0	532.0	11.9	–	–
Cu-Nb ₂ O ₅ _r	207.1	100.0	529.5	19.0	530.3	64.1	531.8	12.9	532.9	3.9
Au-Nb ₂ O ₅ AP	207.2	100.0	528.2	3.1	530.2	65.5	531.5	26.8	533.0	4.6
Au-Nb ₂ O ₅ AP_r	207.0	100.0	528.2	2.6	530.1	62.5	531.6	27.4	532.9	6.5
									533.6	1.1
Au-Nb ₂ O ₅ DR	207.2	100.0	528.4	3.0	530.3	81.7	531.6	15.3	–	–
Au-Nb ₂ O ₅ DR_r	206.9	100.0	527.8	1.9	530.0	71.6	531.6	19.8	533.3	6.7
AuCu-Nb ₂ O ₅ DR	207.1	100.0	529.3	19.2	530.4	72.9	532.1	7.9	–	–
AuCu-Nb ₂ O ₅ DR_r	207.0	100.0	529.5	21.6	530.2	53.4	531.8	18.8	533.2	6.2

^a r – catalyst after photocatalytic reaction.

observed for Au-Nb₂O₅ AP and Au-Nb₂O₅ DR, and was found to be of 84.2 eV. The increase in the binding energy of gold in the bimetallic catalyst confirms that gold strongly interacted with copper species in agreement with the TEM divulgation. This electronic interaction, led to the electron transfer from (Au⁰)^{δ-} to copper species, and resulted in formation of metallic Au NPs without partial negative charge on their surfaces. Fig S10-SD shows the Cu2p XP spectra recorded for Cu-Nb₂O₅ and AuCu-Nb₂O₅ DR catalysts. It was found that for the bimetallic AuCu catalyst, the satellite peaks characteristic of Cu²⁺ species were significantly more intense than for the monometallic ones. Deconvolution of Cu2p XP spectrum of Cu-Nb₂O₅ catalyst allowed us to distinguish two components of Cu species (Table 3): i) at 932.7 eV (88.1%) and ii) at 935.4 eV (11.9%). According to literature [52] the former is characteristic of Cu⁺, while the latter is typical of Cu²⁺ species. Therefore, it was concluded that in Cu-Nb₂O₅ catalyst the majority of copper species were in the form of Cu(I). Deconvolution of Cu2p XP spectrum of the bimetallic AuCu sample permitted us to determine that for this material, the fraction of Cu²⁺ species was significantly greater than for the monometallic catalyst, and was equal to 51.3% of total copper species (Table 3 and Fig S10-SD). The increase in the content of Cu²⁺ species in the bimetallic sample resulted more likely from the presence of gold nanoparticles which catalyzed oxidation of Cu⁺ to Cu²⁺ during the calcination step by a possible electron transfer [53,54]. For both copper catalysts the binding energy of Cu²⁺ species was significantly higher than that reported in literature for unsupported CuO (≈ 933.8 eV [55]). It indicated strong interaction of the niobia support with well dispersed copper species. It is also worth noticing that for the

bimetallic catalyst, the binding energy (BE) of Cu²⁺ species was lower than for the monometallic sample (934.8 eV vs. 935.4 eV for AuCu-Nb₂O₅ DR and Cu-Nb₂O₅, respectively; Table 3). This phenomenon confirmed the presence of strong electronic interaction between gold and copper in the bimetallic catalyst.

Optical properties of the catalysts were studied by UV-vis. Fig. 3 A shows that all materials used in the study exhibited broad and intense absorption band centered at ca. 300 nm, which is characteristic of Nb₂O₅ [10]. Band gap value estimated for pristine niobia support was of 3.18 eV (see Fig. 3 B), and is in agreement with the values of band gaps reported for this semiconductor [10,56]. Deposition of gold on niobia surface led to the appearance of a new broad absorption band with the maximum intensity at ca. 548–573 nm (Fig. 3 A), which is characteristic of surface plasmon resonance (SPR) of metallic gold nanoparticles [57]. The increase in the niobia ability to absorb visible light was also observed for the samples containing copper. As can be seen from UV-vis spectra, modification of niobia with this metal led to an increase in light absorption from ca. 350 nm to ca. 550 nm and from ca. 600 nm to more than 800 nm. According to literature [55,58–63], the above-mentioned absorption bands observed for the catalysts after modification with copper are typical of Cu₂O/CuO phases. The greatest increase in the visible light absorption was observed for the bimetallic gold-copper catalysts, indicating that the presence of strong electronic interaction between gold and copper species (as evidenced by XPS) improved the catalyst ability to absorb visible light.

Acidic properties of catalysts surface can play an important role during the different steps of the photocatalytic reaction (e.g. adsorption

Table 3

State of gold and copper in catalysts before and after methanol photooxidation studied by X-ray photoelectron spectroscopy (binding energies (BEs) normalized to BE of C1 s – 284.8 eV).

Catalyst ^a	Au4f _{7/2}						Cu2p _{3/2}			
	(Au ⁰) ^{δ-}		Au ⁰		Au ^{δ+}		Cu ⁺		Cu ²⁺	
	BE	[%]	BE	[%]	BE	[%]	BE	[%]	BE	[%]
Cu-Nb ₂ O ₅	–	–	–	–	–	–	932.7	88.1	935.4	11.9
Cu-Nb ₂ O ₅ _r	–	–	–	–	–	–	932.5	86.9	934.9	13.1
Au-Nb ₂ O ₅ AP	83.3	100.0	–	–	–	–	–	–	–	–
Au-Nb ₂ O ₅ AP_r	83.2	100.0	–	–	–	–	–	–	–	–
Au-Nb ₂ O ₅ DR	83.3	93.1	–	–	85.0	6.9	–	–	–	–
Au-Nb ₂ O ₅ DR_r	83.0	100.0	–	–	–	–	–	–	–	–
AuCu-Nb ₂ O ₅ DR	–	–	84.2	100.0	–	–	932.8	48.7	934.8	51.3
AuCu-Nb ₂ O ₅ DR_r	–	–	83.9	100.0	–	–	932.5	89.8	935.1	10.2
AuCu-Nb ₂ O ₅ DR_UV	–	–	84.3	100.0	–	–	932.5	87.5	935.3	12.5

^a r – catalyst after photocatalytic reaction; _UV – catalyst irradiated with UV light.

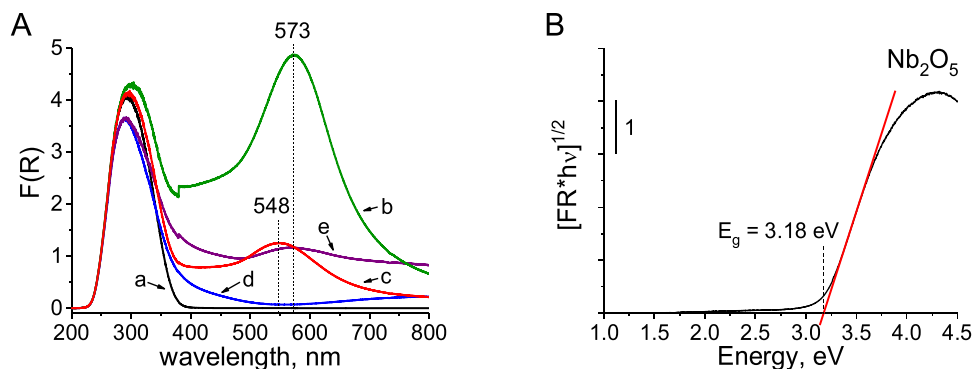


Fig. 3. (A) UV-vis spectra of (a) Nb_2O_5 , (b) $\text{Au}-\text{Nb}_2\text{O}_5$ AP, (c) $\text{Au}-\text{Nb}_2\text{O}_5$ DR, (d) $\text{Cu}-\text{Nb}_2\text{O}_5$ and (e) $\text{AuCu}-\text{Nb}_2\text{O}_5$ DR. (B) Band gap estimation for parent Nb_2O_5 using Tauc's plot method.

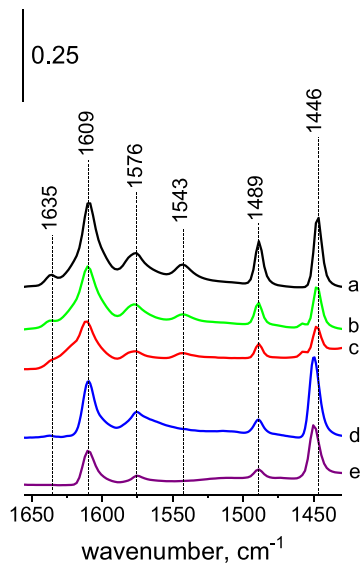


Fig. 4. FTIR spectra of (a) Nb_2O_5 , (b) $\text{Au}-\text{Nb}_2\text{O}_5$ AP, (c) $\text{Au}-\text{Nb}_2\text{O}_5$ DR, (d) $\text{Cu}-\text{Nb}_2\text{O}_5$, (e) $\text{AuCu}-\text{Nb}_2\text{O}_5$ DR after Py adsorption followed by evacuation at 150 °C. The spectra were subtracted from the spectra of the activated samples before Py adsorption and normalized to mass of wafer = 13.0 mg.

of the reactant and products; etc.). These properties were investigated by FTIR spectroscopy combined with pyridine (Py) adsorption as probe. In all the spectra acquired for the catalysts after Py adsorption followed by evacuation at 150 °C (Fig. 4) the bands characteristic of pyridine coordinatively bonded to Lewis acid sites (LAS) (bands at ca. 1609 and 1446 cm^{-1}), pyridine molecules protonated at Brønsted acid sites (BAS) (bands at ca. 1635, 1543 cm^{-1}), and the bands characteristic of both pyridine coordinatively bonded to Lewis acid sites and protonated at Brønsted acid sites (bands at ca. 1576 and 1489 cm^{-1}) were observed [64–66]. In order to compare the acidity of the catalysts, the number of BAS and LAS was estimated from the surface area of the bands characteristic of pyridine chemisorbed on BAS (ca. 1543 cm^{-1}) and LAS (ca. 1446 cm^{-1}) using the extinction coefficients of 1.20 $\mu\text{mol}\cdot\text{cm}^{-1}$ and 3.15 $\mu\text{mol}\cdot\text{cm}^{-1}$ for Brønsted and Lewis acid sites, respectively [33,67]. As can be seen from Table 1, deposition of gold on the surface of Nb_2O_5 significantly reduced the number of BAS, while the deposition of copper led to almost total disappearance of Brønsted acidity. The decrease in the acidity of $\text{AuCu}-\text{Nb}_2\text{O}_5$ DR was the greatest due to the highest concentration of modifiers. It was also observed that the gold deposition affected not only the concentration of BAS, but also significantly reduced the Lewis acidity of niobia. The decrease in the concentration of LAS did not occur in the catalyst that was modified with both gold and copper. Table 1 shows that the number of LAS estimated for $\text{AuCu}-\text{Nb}_2\text{O}_5$ DR was significantly greater than for $\text{Au}-\text{Nb}_2\text{O}_5$ AP, $\text{Au}-\text{Nb}_2\text{O}_5$

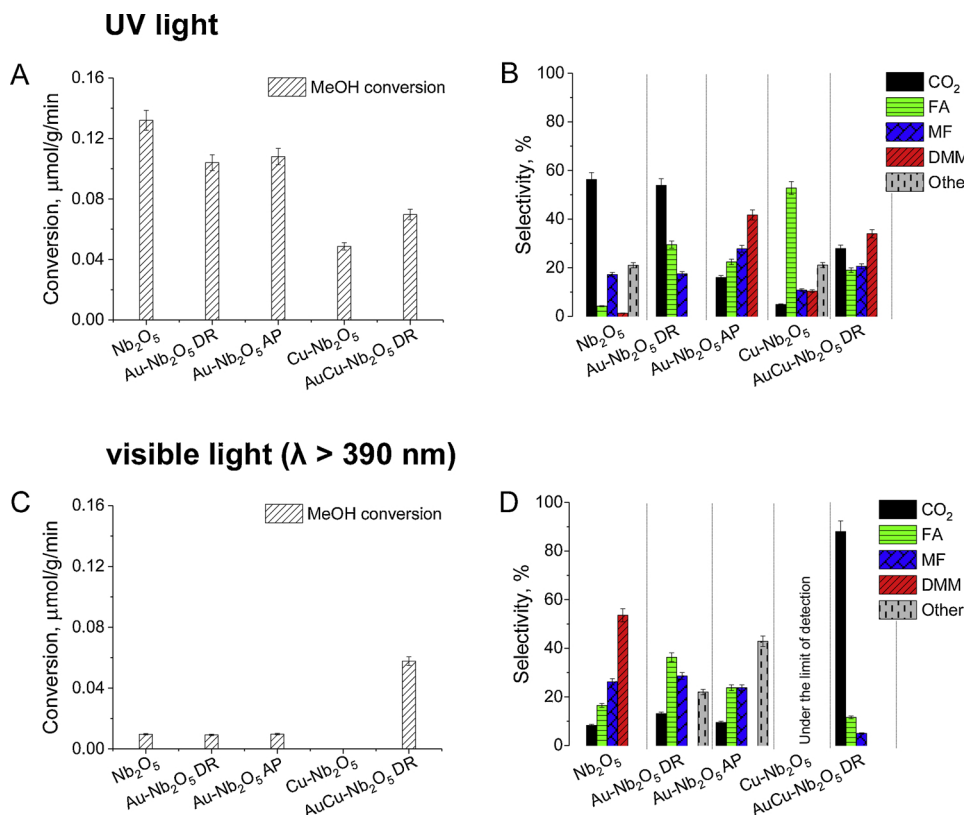
DR and pristine Nb_2O_5 . The greatest number of LAS was observed on the surface of $\text{Cu}-\text{Nb}_2\text{O}_5$. This indicated that the deposition of copper led to the formation of new LAS on the surface of the catalysts. It is in agreement with the results of XPS studies which revealed that copper in the catalysts existed in the form of Cu^+ and Cu^{2+} species (Table 3 and Fig. S10-SD).

3.2. Catalytic activity in methanol photooxidation

Photocatalytic activity of the materials was tested in gas phase methanol oxidation under different reaction conditions (detailed methodology of methanol oxidation is described in the experimental part; see Section 2.3). All photocatalytic tests were performed under flow condition during few hours. No significant deactivation was observed for all samples over the reaction time.

The results of selected photocatalytic tests are summarized in Fig. 5. It is clear that chemical composition of the photocatalysts has significant impact on their properties. The highest activity under high intensity UV light irradiation was characteristic of unmodified Nb_2O_5 (see Fig. 5 A). Deposition of gold and/or copper species reduced significantly the niobia activity. The highest decrease in the activity of Nb_2O_5 was observed for the samples modified with copper, i.e. $\text{Cu}-\text{Nb}_2\text{O}_5$ and $\text{AuCu}-\text{Nb}_2\text{O}_5$ DR. Besides the chemical composition of the materials, the nature of light source (UV vs. visible) was found to be another factor that has significant impact on the photocatalysts performance. As can be seen in Fig. 5 C, under irradiation with visible light unmodified niobia and all monometallic samples exhibited marginal activity. However, remarkable activity was observed over the bimetallic $\text{Au}-\text{Cu}$ catalyst under visible light at the same reaction conditions. It was found that this catalyst was much more active than the rest of the materials and exhibited almost the same methanol conversion as that observed under the irradiation with high intensity UV light (Fig. 5 A and C).

Fig. 5 B shows that chemical composition and surface properties of the materials used in this study affected not only the activity, but also the selectivity. Of course, direct comparison of the selectivity of all the catalysts shown in Fig. 5 B is not possible due to different methanol conversions, but some important differences can be easily found. As can be seen from Fig. 5 B, very interesting variations in the catalysts selectivity at similar methanol conversions were observed for monometallic gold catalysts prepared by different synthesis routes. The catalyst prepared by the deposition-reduction method ($\text{Au}-\text{Nb}_2\text{O}_5$ DR) was found to be highly active in total oxidation of methanol (the amount of CO_2 in the products was greater than 50%), while the catalyst prepared by anchoring of gold on the surface of niobia grafted with APTMS ($\text{Au}-\text{Nb}_2\text{O}_5$ AP) exhibited high selectivity to DMM (its selectivity to DMM was of 41.7%) under UV irradiation condition. Interesting variations in the catalysts selectivity were also observed for $\text{Cu}-\text{Nb}_2\text{O}_5$ and $\text{AuCu}-\text{Nb}_2\text{O}_5$ DR. Addition of gold to $\text{Cu}-\text{Nb}_2\text{O}_5$ brought a significant



enhancement of the catalyst ability to total oxidation of methanol (percentage of carbon dioxide in the products of methanol photo-oxidation over $\text{Cu-Nb}_2\text{O}_5$ and $\text{AuCu-Nb}_2\text{O}_5$ DR was found to be of 4.9% and 27.9%, respectively) and further transformation of formaldehyde to MF and DMM (see Fig. 5 B).

As far as selectivity is concerned, it was also documented that the nature of the light source is another factor that had significant impact on the products distribution in methanol photooxidation. As can be seen from Fig. 5, visible light irradiation promoted total oxidation of methanol over $\text{AuCu-Nb}_2\text{O}_5$ DR catalyst (see Fig. 5 D), while the same catalyst suffered from low selectivity under high intensity UV light irradiation (see Fig. 5 B).

3.3. Oxidation state of metals after the photocatalytic reactions

In order to evaluate changes in the oxidation state of metals after photocatalytic reactions, the catalysts were characterized with the use of X-ray photoelectron spectroscopy (results of XPS studies are shown in Tables 2 and 3, and Figs. S11-S14-SD). As can be seen from Tables 2 and 3, the oxidation states of niobium and gold after the photocatalytic processes were not significantly changed. Analysis of oxygen XP spectra showed that in all catalysts after methanol oxidation, the amount of surface hydroxyl groups and fraction of O_{IV} species characteristic of oxygen in organic compounds ($\text{C}-\text{O}$ and/or $\text{C}=\text{O}$) slightly increased. The increase in the number of the surface hydroxyl groups can be related to the abstraction of hydrogen from the adsorbed methanol/reaction products (mainly H_2O) by nucleophilic oxygen species present on the surface of the catalysts. Moreover, the increase in the fraction of oxygen in organic compounds results from the presence of unreacted substrates, reaction intermediates and/or products adsorbed on the catalysts. The most significant changes took place on the surface of the bimetallic catalyst, i.e. $\text{AuCu-Nb}_2\text{O}_5$ DR. For this material a significant reduction of Cu^{2+} to Cu^+ species was observed (Table 3, Fig. S13-SD). In order to investigate whether the reduction of copper species occurred during the pre-irradiation step or during the photocatalytic reaction,

Fig. 5. Activity (A, C) and selectivity (B, D) of the catalysts at the steady state during the photocatalytic oxidation of methanol under high intensity UV irradiation (irradiance $\approx 205\text{ mW/cm}^2$; 4th step of the reaction procedure, see experimental section) and visible light irradiation ($\lambda > 390\text{ nm}$; irradiance $\approx 190\text{ mW/cm}^2$; 6th step of the reaction procedure, see experimental section).

the bimetallic catalyst was irradiated with UV light, and then the oxidation state of the metals was analyzed by X-ray photoelectron spectroscopy. It was found that the irradiation of $\text{AuCu-Nb}_2\text{O}_5$ DR with UV light resulted in a significant reduction of Cu^{2+} to Cu^+ (see Table 3 and Fig. S13-SD). This observation allowed drawing the conclusion that the Cu^{2+} species were reduced to Cu^+ during the pre-irradiation step, not during the photocatalytic reaction.

3.4. Discussion on the factors determining activity and selectivity of niobia-based catalysts in methanol photooxidation

3.4.1. Factors determining the activity of the catalysts

Doping of semiconductors with various metals is one of the most promising strategies for the improvement of photocatalytic activity of semiconductors. Hitherto, many authors have reported that modification of ZnO [68,69] or TiO_2 [11] with gold led to significant increase in the photocatalysts performance. In view of these results, one can expect that modification of niobia with gold and/or copper should improve the activity of Nb_2O_5 . However, the results obtained in this study clearly show that doping of niobia with the metals reduces the activity of the catalysts under UV light (see Fig. 5 A).

As can be seen from Table 1, one of the most important differences in the surface properties of the catalysts are their Brønsted and Lewis acidities. In order to demonstrate the impact of the above-mentioned parameter on the photocatalytic activity of materials, a graph of the number of BAS/LAS against methanol conversion over different samples was plotted in Fig. 6A and B. It was found that there was some linear relationship between the number of LAS on the surface of $\text{Au-Nb}_2\text{O}_5$ DR, $\text{Au-Nb}_2\text{O}_5$ AP and Nb_2O_5 and their photocatalytic activity, but this tendency was impeded by addition of copper dopant (see Fig. 6A). The undisputable linear trend was observed for the graph presenting the relationship between the number of Brønsted acid sites versus the methanol conversion. Fig. 6B clearly shows that the greater the amount of BAS on the surface of the photocatalyst, the higher the catalyst activity in methanol oxidation. According to literature [2], the

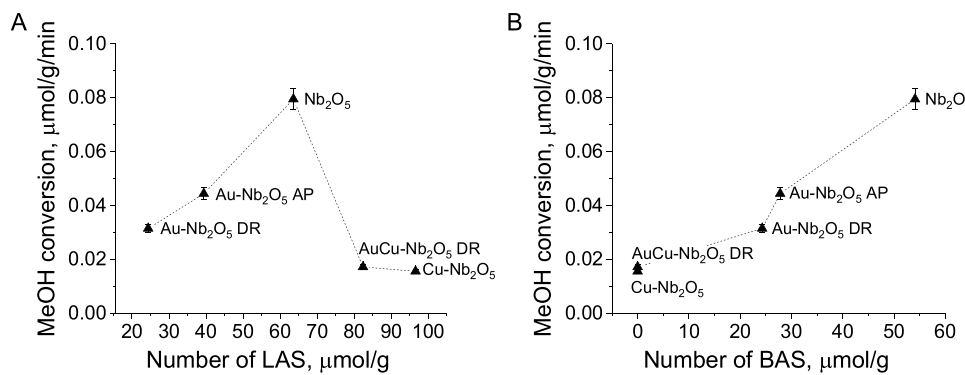


Fig. 6. The influence of Lewis (A) and Brønsted (B) acidity of the catalysts on their activity in methanol photooxidation (UV light with moderate intensity, light intensity $\approx 70 \text{ mW/cm}^2$, 5th step of the reaction procedure, see experimental section).

first step in the photocatalytic oxidation of methanol is formation of surface methoxy species. Acidic sites take part in the dissociative chemisorption of methanol towards methoxy species. The as-formed methoxy species can be then oxidized by photogenerated holes to yield formaldehyde and/or other products. Thus, one can expect that high concentration of Brønsted/Lewis acidic sites on the catalyst promoted formation of a greater number of methoxy species on the photocatalyst surface, and this resulted in higher photocatalytic activity of materials in methanol oxidation. Indeed, high Brønsted/Lewis acidity of unmodified niobia (see Table 1), much higher than that observed for Au-Nb₂O₅ AP and Au-Nb₂O₅ DR, resulted in higher concentration of methoxy species on the surface of unmodified niobium pentoxide (see Fig. S17-SD) and this allowed higher methanol conversion over pristine Nb₂O₅ (see Fig. 6A and B). Similar relationship between the activity of the catalysts and their acidity was also found for monometallic gold catalysts. As can be seen from Fig. 6A and B, Au-Nb₂O₅ AP had higher number of Brønsted and Lewis acidic sites than Au-Nb₂O₅ DR and was more active in methanol photooxidation than the latter catalyst. It is important to notice that Cu-Nb₂O₅ sample did not follow the above-mentioned tendency. As can be seen from Fig. S17-SD, Cu-Nb₂O₅ had similar concentration of surface methoxy species (IR bands at ca. 2927 and 2829 cm^{-1}) as unmodified niobia but was less active than Nb₂O₅. This phenomenon can be explained by the shading effect of Cu dopant [70,71]. Fig. 3 clearly shows that deposition of copper on niobia led to significant decrease in light absorption at ca. 300 nm which is characteristic of bulk Nb₂O₅.

Another important factor determining the catalysts activity in methanol photooxidation was the nature of light source (in other words, the nature of the excited active sites). Under high intensity UV light irradiation, the highest activity was observed for unmodified niobia, but under the visible light this metal oxide exhibited marginal activity (see Fig. 5). This phenomenon resulted from the fact that under visible light niobia could not be efficiently activated due to its large band gap ($E_g = 3.18 \text{ eV}$; Fig. 3). As can be seen from Fig. 5 C, the activity of niobia under visible light irradiation was not enhanced even after deposition of plasmonic Au NPs (Au-Nb₂O₅ AP and Au-Nb₂O₅ DR) or copper/cupric oxide species (Cu-Nb₂O₅). It showed that both copper and gold alone cannot activate niobia under visible light irradiation, although both metals exhibit the ability to absorb visible light (see UV-vis spectra of catalysts; Fig. 3). However, the presence of both gold and copper on the surface of niobium pentoxide (AuCu-Nb₂O₅ DR) brought about high catalytic activity under visible light irradiation, much higher than in the monometallic catalysts. This observation led to the conclusion that above-mentioned enhancement of catalytic activity of the bimetallic catalyst under visible light irradiation had to result from the presence of strong interaction between gold and copper, which was evidenced by XPS. As can be seen from the UV-vis spectra (see Fig. 3), the presence of this strong interaction between gold and copper in the bimetallic sample significantly improved the catalyst ability to

absorb visible light. We established that the above-mentioned increase in the catalytic activity of niobia after deposition of both gold and copper can be explained by the improved plasmonic energy transfer and enhanced charge separation from photoexcited gold nanoparticles to copper/cupric oxide species. According to Wu [72], the plasmonic energy transfer can proceed through three different mechanisms: (i) light scattering/trapping, (ii) plasmon-induced resonance energy transfer (PIRET), and (iii) hot electron injection, also known as direct electron transfer (DET). Since light scattering process is typical of large gold nanoparticles (typically larger than 50 nm in diameter) [72], a significant role of this mechanism can be excluded in the present study. The latter two mechanisms, i.e. plasmon-induced resonance energy transfer and hot electron injection process are very likely and it is difficult to conclude which one is dominant. The enhancement of catalytic activity of Ag@Cu₂O core-shell structures under visible light irradiation through mixed DET and PIRET mechanisms, has been earlier reported by Li et al. [73]. Hitherto, the positive effect of Au-Cu₂O interaction on the activity of materials in photocatalytic water splitting has been also observed by Zhang et al. [17]. However, Zhang et al. [17] proposed another explanation of the enhancement of Cu₂O activity after gold deposition. They inferred that an increase in visible light activity of Au/Cu₂O heterostructures resulted from enhanced separation of electrons and holes generated in Cu₂O under light irradiation. It cannot be excluded that in the present study, gold acted both as an electron sink increasing the efficiency of photogenerated charge carriers separation and as a component which enhanced the ability of Cu₂O/CuO to generate photoexcited electrons and holes due to plasmon energy transfer from Au NPs to the semiconductor. The explanation of this mechanisms requires further study with appropriate techniques.

3.4.2. Factors determining the catalysts selectivity

3.4.2.1. The influence of the catalysts acidity. The results obtained in this study clearly show that the surface properties of materials not only affect the photocatalysts performance, but have also significant influence on the selectivity of the reaction. Monometallic gold catalysts, having similar chemical composition but various concentration of BAS and LAS on the catalysts surfaces, exhibited totally different selectivity in methanol oxidation. *Operando*-IR studies led us to conclude that the differences in the selectivity of Au-Nb₂O₅ AP and Au-Nb₂O₅ DR resulted from different reaction pathways. It was found that methanol photooxidation over the catalyst with lower number of BAS and LAS (i.e. Au-Nb₂O₅ DR) proceeded through dioxomethylene intermediate. As can be seen from Figs. 7 and S21-SD, the vibrational band characteristic of this intermediate product (IR band at ca. 2876 cm^{-1} [74,75]) was immediately formed after the high intensity UV light irradiation (4th step of the reaction procedure, see experimental section). It is important to note that carbon dioxide was the main product of the reaction in which dioxomethylene intermediate was identified (see Fig. 5B). For Au-Nb₂O₅ AP (a higher number of BAS

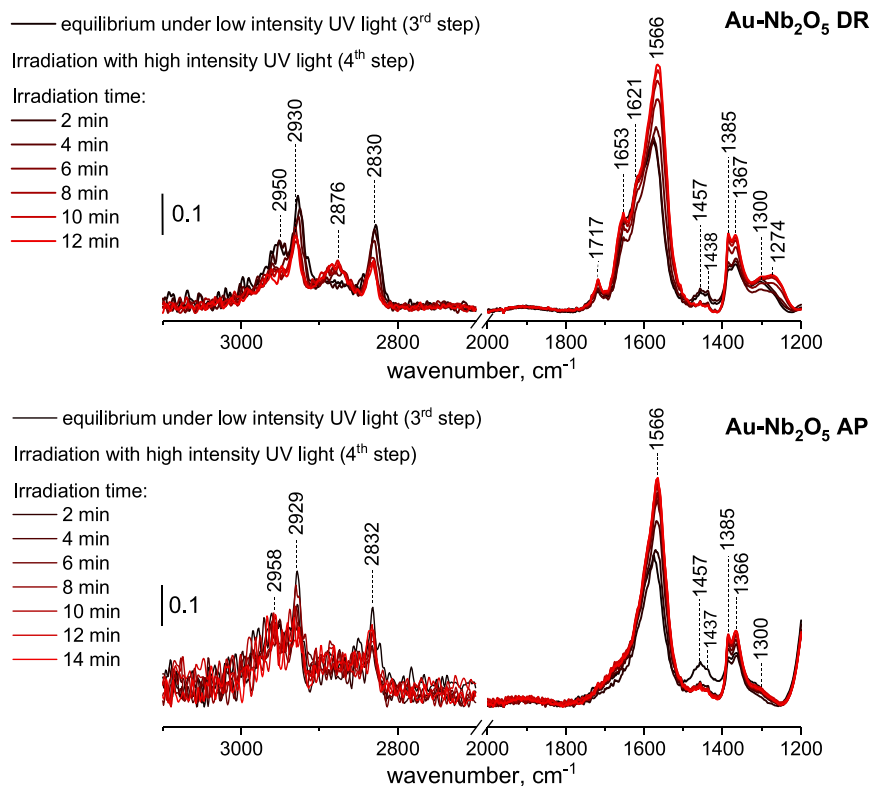
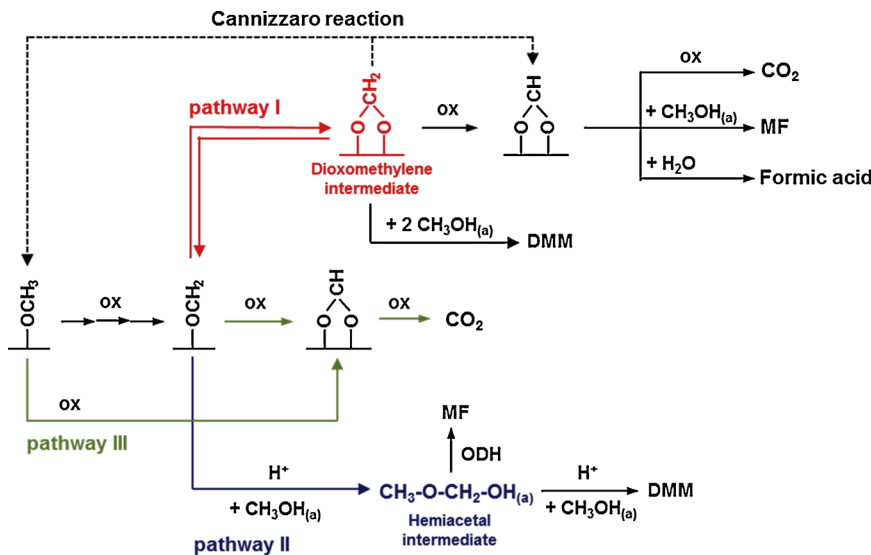


Fig. 7. IR spectra of the adsorbed surface species on Au-Nb₂O₅ DR and Au-Nb₂O₅ AP during the first minutes of irradiation with high intensity UV light (light intensity $\approx 205 \text{ mW/cm}^2$; 4th step of the reaction procedure, see experimental section).



Scheme 2. Proposed reaction pathway estimated on the basis of literature [1,2,82,3,6,74–79] and results of this study. DMM – dimethoxymethane; MF – methyl formate; ox – oxidation reaction; (a) – adsorbed; ODH – oxidative dehydrogenation.

and LAS), the dioxomethylene intermediate was not observed and the main reaction product was dimethoxymethane. There are two possible explanations of the lack of dioxomethylene intermediate on the surface of Au-Nb₂O₅ AP. The first assumes that formation of dioxomethylene species is followed by their very fast consumption caused by the reaction with molecularly adsorbed methanol molecules to yield dimethoxymethane [74,76] (see Scheme 2, pathway I). The second explanation assumes that the oxidation of methanol over Au-Nb₂O₅ AP did not proceed through dioxomethylene intermediate, but through condensation of formaldehyde with adsorbed methanol to yield hemiacetal intermediate (see Scheme 2, pathway II) [77]. This

hemiacetal intermediate undergoes then intermolecular dehydration with another methanol molecule leading to formation of DMM [77,78]. Since Au-Nb₂O₅ AP exhibited higher Brønsted acidity and higher concentration of molecularly adsorbed methanol on the catalyst surface than that observed for Au-Nb₂O₅ DR (see Fig. S20-SD), the oxidation of methanol through hemiacetal intermediate over the former catalyst is very likely. Hemiacetal intermediate could not be observed in the FTIR spectra of Au-Nb₂O₅ AP because of its very low stability. Li et al. [78] have revealed that this intermediate product is readily transformed into methyl formate or dimethoxymethane, depending on the reaction conditions.

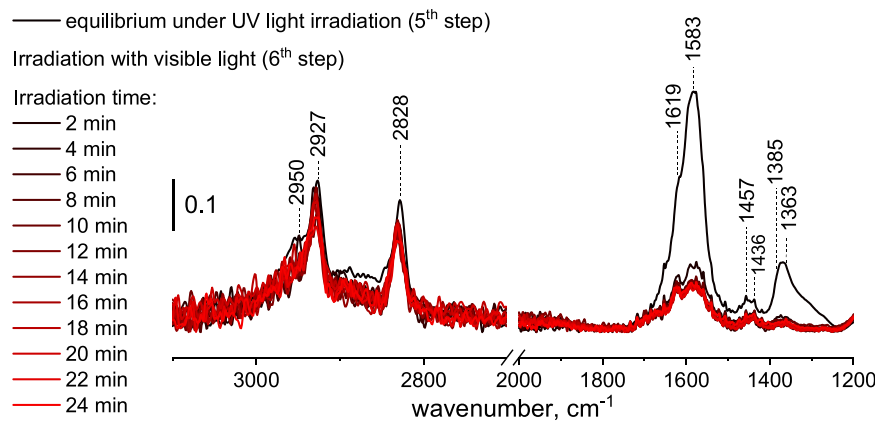


Fig. 8. IR spectra of the adsorbed surface species on AuCu-Nb₂O₅ DR during the first minutes of irradiation with visible light ($\lambda > 390$ nm; light intensity $\approx 190 \text{ mW/cm}^2$; 6th step of the reaction procedure, see experimental section).

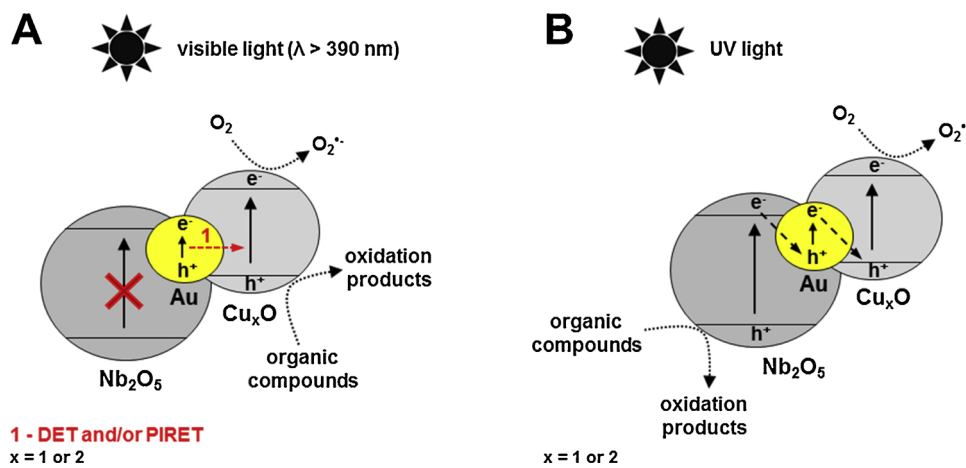
The differences in the reaction pathways over Au-Nb₂O₅ AP and Au-Nb₂O₅ DR were also concluded from the analysis of FTIR surface spectra of the catalysts in the range of 2000–1200 cm^{-1} . As can be seen in Fig. 7, one of the products of methanol photooxidation over Au-Nb₂O₅ DR were the surface species characterized by the IR band at ca. 1653 cm^{-1} , which is typical of adsorbed methyl formate [74]. According to literature [79], methyl formate can be formed as a product of the reaction between bidentate formate species and adsorbed methanol. As can be seen from Fig. S21-SD, Au-Nb₂O₅ DR had much more formate species on its surface than Au-Nb₂O₅ AP, and this probably resulted in a higher selectivity of the former catalyst toward formation of MF. We established that bidentate formate species on the surface of Au-Nb₂O₅ DR catalyst were more likely to be formed by oxidation of dioxomethylene intermediate (see Scheme 2, pathway I) [75]. The as-formed bidentate formate species reacted then with adsorbed methanol (methoxy) to yield MF or were further oxidized to CO₂, depending on the reaction conditions.

If the above proposed pathway of MF formation over Au-Nb₂O₅ DR catalyst is correct, at low methanol conversion this catalyst should exhibit high selectivity to MF. Indeed, Fig. S22-SD shows that under low intensity monochromatic UV light applied in the 3rd step of experiment procedure (leading to low activity) the selectivity of Au-Nb₂O₅ DR catalyst to MF was of 51.7%. Moreover, high methanol conversion (low concentration of adsorbed methanol molecules) should promote total oxidation of surface formate species over Au-Nb₂O₅ DR catalyst. As can be seen from Fig. 5 B, the main product of methanol oxidation over Au-Nb₂O₅ DR under high intensity UV irradiance was CO₂.

All these observations allowed drawing the conclusion that the reaction pathway through dioxomethylene intermediate over the gold catalyst prepared by deposition-reduction method is very likely. It is important to stress that above-described relationship between the methanol conversion and the catalyst selectivity to MF was not observed for Au-Nb₂O₅ AP, for which dioxomethylene intermediate was not identified. As can be seen from Fig. S22-SD, under low intensity monochromatic UV light, Au-Nb₂O₅ AP was highly selective to DMM (the amount of MF in the products was negligible). The increase in methanol conversion under high intensity UV irradiance decreased by a half the catalyst selectivity to DMM, but did not lead to total disappearance of this product, as it was observed for Au-Nb₂O₅ DR (see Fig. 5 B). It is also important to notice that the decrease in selectivity of Au-Nb₂O₅ AP to DMM was associated with the increase in the catalyst selectivity to MF, not to CO₂, as found for Au-Nb₂O₅ DR. In view of these results, we claim that the increase in the selectivity of Au-Nb₂O₅ AP to MF resulted more likely from oxidative dehydrogenation of hemiacetal intermediate rather than from the reaction of surface formate species with adsorbed methanol molecules (see Scheme 2, pathway II).

Fig. 7 also shows that there is one more important difference in the composition of the catalyst surfaces during the methanol photooxidation under high intensity UV light irradiation. Only in the FTIR spectrum of Au-Nb₂O₅ DR, an additional vibration band at ca. 1717 cm^{-1} characteristic of adsorbed formaldehyde was observed [26]. One can expect that formaldehyde is stronger adsorbed on the surface of the catalyst prepared by deposition-reduction method, and thus this product can be easily transformed into dioxomethylene intermediate, and then further oxidized to methyl formate or CO₂. Another possible hypothesis assumes that formaldehyde adsorbed on the surface of Au-Nb₂O₅ AP is immediately transformed into hemiacetal intermediate through the reaction with molecularly adsorbed methanol (see Scheme 2, pathway II). Since Au-Nb₂O₅ AP had more molecularly adsorbed methanol on the catalyst surface (see Fig. S20-SD) and more BAS which play an important role in DMM formation, the latter hypothesis is very likely. If this hypothesis is correct, at low methanol conversion (i.e. at high concentration of molecularly adsorbed methanol on the catalyst surface), Au-Nb₂O₅ AP should exhibit high selectivity to DMM. Indeed, the experiment with the use of low intensity monochromatic UV light ($\lambda = 365$ nm) confirms that at low methanol conversion the selectivity of the catalyst to DMM was very high (ca. 85% selectivity to DMM; Fig. S22-SD).

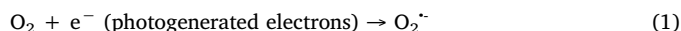
3.4.2.2. The influence of light source on selectivity. Methanol photooxidation over AuCu-Nb₂O₅ DR catalyst using different light sources (UV vs. visible) showed that the nature of the light is another factor that has a significant impact on the selectivity. It was found that under high intensity UV light, methanol was selectively oxidized to MF, FA and DMM (see Fig. 5 B), while visible light promoted total oxidation of the alcohol (see Fig. 5 D). *Operando*-IR studies permitted us to observe that the differences in the catalyst selectivity under UV and visible light resulted more likely from different reaction pathways. It was found that methanol photooxidation under visible light proceeded through the pathway in which all the intermediate products, such as formate species, are immediately consumed to yield CO₂ without formation of significant amount of intermediate products (Fig. 8 clearly shows that the intensity of the bands characteristic of surface formate species (band at ca. 1583 cm^{-1}) decreased significantly when the light source was changed from UV to visible). In view of these observations, we have proposed the possible mechanism for total oxidation of methanol under visible light irradiation over AuCu-Nb₂O₅ DR (see Scheme 3A). It is known that niobium pentoxide cannot be excited effectively under visible light irradiation due to its wide band gap. Therefore, under visible light, the oxidation of methanol had to proceed mainly with the use of Cu₂O/CuO and/or Au as active components. As mentioned in the previous section, in the Au-Cu₂O heterostructures gold nanoparticles can enhance both



Scheme 3. Mechanism of photocatalytic process determined on the basis of literature [12,81,83,84] and results obtained in this study.

generation and separation of photoexcited electrons and holes in Cu_2O under visible irradiation. Since unmodified niobia could not be efficiently activated under such reaction conditions and gold can significantly enhance the photocatalytic activity of $\text{Cu}_2\text{O}/\text{CuO}$, we concluded that under visible light methanol was oxidized by positively charged holes (h^+) localized in the valence band of $\text{Cu}_2\text{O}/\text{CuO}$ (Scheme 3A). A very important factor promoting total oxidation of methanol over $\text{AuCu-Nb}_2\text{O}_5$ DR under visible light was formation of superoxide radical anions on the surface of $\text{Cu}_2\text{O}/\text{CuO}$, i.e. at the same active sites at which the oxidation of organic compounds by photogenerated holes took place (see Scheme 3A).

According to earlier reports, surface methoxy species and adsorbed methanol molecules can be directly oxidized by superoxide radical anions (formed in reaction (1)) to yield bidentate formate species (reaction (2)) [3], which can further react with photogenerated holes (h^+) to yield formyloxy radical followed by its total oxidation to CO_2 (reactions (3) and (4)) [75].



Therefore, it is very likely that formation of superoxide radical anions in a close proximity to methoxy species adsorbed on the surface of $\text{Cu}_2\text{O}/\text{CuO}$ (as shown in Scheme 3A) promoted the total oxidation pathway over the bimetallic $\text{AuCu-Nb}_2\text{O}_5$ DR catalyst. On the other hand, under UV light irradiation, all components of the catalyst (i.e. Au, Nb_2O_5 , $\text{Cu}_2\text{O}/\text{CuO}$) were excited. We established that under such conditions photooxidation of methanol proceeded through all-solid-state (ASS) Z-scheme mechanism [80] shown in Scheme 3B. The photogenerated electrons from conduction band of Nb_2O_5 were transferred through Au nanoparticles to $\text{Cu}_2\text{O}/\text{CuO}$, where they recombined with photogenerated holes localized in valence band of $\text{Cu}_2\text{O}/\text{CuO}$. This process resulted in accumulation of positively charged holes in the valence band of Nb_2O_5 , and photoexcited electrons in the conduction band of $\text{Cu}_2\text{O}/\text{CuO}$ (accumulation of photoexcited electrons in the copper species is in agreement with reduction of CuO to Cu_2O after the irradiation with UV light; see Table 3). The photogenerated holes localized in the valence band of Nb_2O_5 were then accepted by adsorbed organic compounds leading to their oxidation, while the electrons localized in the conduction band of $\text{Cu}_2\text{O}/\text{CuO}$ were accepted by electron acceptors, such as O_2 leading to superoxide radical anions. Under UV irradiation, the oxidation of methanol took place on the surface of Nb_2O_5 (not on the surface of $\text{Cu}_2\text{O}/\text{CuO}$ as under visible light irradiation), which exhibited significantly higher ability to form surface

methoxy species than $\text{Cu}_2\text{O}/\text{CuO}$ (see Fig. S17-SD). High concentration of surface methoxy species on niobium pentoxide and separation of oxygen radicals located on $\text{Cu}_2\text{O}/\text{CuO}$ promoted formation of products of partial oxidation, such as formaldehyde, methyl formate and dimethoxymethane. Similar variations in the selectivity of multi-component photocatalysts under different light sources have been also observed by other authors (e.g. [12] and [81]).

4. Conclusions

The results obtained in this study clearly show that the activity of niobia-based catalysts under UV light is strongly affected by the number of Brønsted/Lewis acid sites on their surfaces. It was documented that deposition of metals (Au and/or Cu) reduced the amount of BAS/LAS on niobia surface, and this decreased the catalysts activity in methanol photooxidation. The opposite behavior was observed in the reaction performed under visible light, in which modification of niobia with both gold and copper species allowed high activity in methanol oxidation, much higher than that observed for unmodified niobia and the other monometallic catalysts. Such a significant increase in the activity of the bimetallic catalyst resulted from the strong interaction between gold and copper species which modified the optical and photocatalytic properties of the catalyst surface.

As far as the catalysts selectivity is concerned, it was documented that one of the key factors determining the distribution of the products of methanol oxidation under UV light are acidic properties of the photocatalyst surface and mechanism of the photocatalytic process. Very important role played the separation of superoxide radical anions from the reaction substrates and/or intermediate products. When superoxide radical anions were formed in a close proximity to reaction substrates/intermediate products, high catalysts ability to total oxidation of methanol was observed.

Finally, it was documented that the nature of light source (UV vs. visible) has remarkable influence on the activation of catalysts components, and thus on the reaction mechanism. In the case of the bimetallic $\text{AuCu-Nb}_2\text{O}_5$ DR, visible light selectively activated gold and copper species, and this promoted total oxidation of methanol. On the other hand, irradiation of $\text{AuCu-Nb}_2\text{O}_5$ DR catalyst with UV light activated all the catalyst components (i.e. gold, copper and niobium species) which resulted in modification of the reaction mechanism and led to formation of significant amount of selective oxidation products, i.e. FA, MF and DMM.

Detailed analysis and discussion of possible reaction mechanisms and pathways described in this paper allowed understanding of the influence of the nature of light source and surface properties of catalysts on their activity and selectivity in photocatalytic oxidation of methanol. This fundamental knowledge on the mechanism of photocatalytic

processes over supported metal catalysts can have significant impact on the development of new catalysts effective in environmentally friendly processes for the removal of methanol from the air pollutions or transformation of this alcohol into other, more valuable products.

Acknowledgements

This work was supported by the National Science Centre, Poland (Grant No. 2018/28/C/ST5/00255) and Erasmus + exchange programme. Lukasz Wolski wishes to thank Mr. Nicolas Sadovnik from LSC Caen, France, for his assistance in FTIR *in situ* measurements.

Part of the research was carried out using the equipment purchased with the funds from the European Regional Development Fund in the framework of the Polish Innovation Economy Operational Program (Contract No. POIG.02.01.00-12-023/08).

Appendix A. Supplementary data

Supplementary material related to this article can be found, in the online version, at <https://doi.org/10.1016/j.apcatb.2019.117978>.

References

- A.S. Crampton, L. Cai, N. Janvelyan, X. Zheng, C.M. Friend, Methanol photo-oxidation on rutile TiO₂ nanowires: probing reaction pathways on complex materials, *J. Phys. Chem. C* 121 (2017) 9910–9919, <https://doi.org/10.1021/acs.jpcc.7b01385>.
- D.A. Panayotov, S.P. Burrows, J.R. Morris, Photooxidation mechanism of methanol on rutile TiO₂ nanoparticles, *J. Phys. Chem. C* 116 (2012) 6623–6635, <https://doi.org/10.1021/jp209215c>.
- M. El-Roz, P. Bazin, F. Thibault-Starzyk, An operando-IR study of photocatalytic reaction of methanol on new *BEA supported TiO₂ catalyst, *Catal. Today* 205 (2013) 111–119, <https://doi.org/10.1016/j.cattod.2012.08.023>.
- M. El-Roz, M. Kus, P. Cool, F. Thibault-Starzyk, New operando IR technique to study the photocatalytic activity and selectivity of TiO₂ nanotubes in air purification: influence of temperature, UV intensity, and VOC concentration, *J. Phys. Chem. C* 116 (2012) 13252–13263, <https://doi.org/10.1021/jp3034819>.
- M. El-Roz, L. Lakiss, I. Telegeiev, O.I. Lebedev, P. Bazin, A. Vicente, C. Fernandez, V. Valtchev, High-visible-light photoactivity of plasma-promoted vanadium clusters on nanozeolites for partial photooxidation of methanol, *ACS Appl. Mater. Interfaces* 9 (2017) 17846–17855, <https://doi.org/10.1021/acsami.7b02161>.
- M. El-Roz, P. Bazin, M. Daturi, F. Thibault-Starzyk, On the mechanism of methanol photooxidation to methylformate and carbon dioxide on TiO₂: an operando-FTIR study, *Phys. Chem. Chem. Phys.* 17 (2015) 11277–11283, <https://doi.org/10.1039/C5CP00726G>.
- M. El-Roz, P. Bazin, M. Daturi, F. Thibault-Starzyk, Operando IR coupled to SSITKA for photocatalysis: reactivity and mechanistic studies, *ACS Catal.* 3 (2013) 2790–2798, <https://doi.org/10.1021/cs4006088>.
- S. Rehman, R. Ullah, A.M. Butt, N.D. Gohar, Strategies of making TiO₂ and ZnO visible light active, *J. Hazard. Mater.* 170 (2009) 560–569, <https://doi.org/10.1016/j.jhazmat.2009.05.064>.
- H. Sun, S. Liu, S. Liu, S. Wang, A comparative study of reduced graphene oxide modified TiO₂, ZnO and Ta₂O₅ in visible light photocatalytic/photocatalytic oxidation of methylene blue, *Appl. Catal. B Environ.* 146 (2014) 162–168, <https://doi.org/10.1016/j.apcatb.2013.03.027>.
- T. Sreethawong, S. Ngamsinlapasathian, S. Yoshikawa, Crystalline mesoporous Nb₂O₅ nanoparticles synthesized via a surfactant-modified sol-gel process, *Mater. Lett.* 78 (2012) 135–138, <https://doi.org/10.1016/J.Matlet.2012.03.045>.
- P.A. DeSario, J.J. Pietron, D.E. Devantier, T.H. Brintlinger, R.M. Stroud, D.R. Rolison, Plasmonic enhancement of visible-light water splitting with Au-TiO₂ composite aerogels, *Nanoscale* 5 (2013) 8073–8083, <https://doi.org/10.1039/c3nr01429k>.
- X. Wang, H. Dong, Z. Hu, Z. Qi, L. Li, Fabrication of a Cu₂O/Au/TiO₂ composite film for efficient photocatalytic hydrogen production from aqueous solution of methanol and glucose, *Mater. Sci. Eng. B Solid-State Mater. Adv. Technol.* 219 (2017) 10–19, <https://doi.org/10.1016/j.mseb.2017.02.011>.
- X. Lang, X. Chen, J. Zhao, Heterogeneous visible light photocatalysis for selective organic transformations, *Chem. Soc. Rev.* 43 (2014) 473–486, <https://doi.org/10.1039/c3cs60118a>.
- S. Sarina, E.R. Waclawik, H. Zhu, Photocatalysis on supported gold and silver nanoparticles under ultraviolet and visible light irradiation, *Green Chem.* 15 (2013) 1814–1833, <https://doi.org/10.1039/c3gc40450a>.
- J. Wang, G. Ji, Y. Liu, M.A. Gondal, X. Chang, Cu₂O/TiO₂ heterostructure nanotube arrays prepared by an electrodeposition method exhibiting enhanced photocatalytic activity for CO₂ reduction to methanol, *Catal. Commun.* 46 (2014) 17–21, <https://doi.org/10.1016/j.catcom.2013.11.011>.
- D.P. DePuccio, C.C. Landry, Photocatalytic oxidation of methanol using porous Au/WO₃ and visible light, *Catal. Sci. Technol.* 6 (2016) 7512–7520, <https://doi.org/10.1039/C6CY01449F>.
- W. Zhang, B. Wang, C. Hao, Y. Liang, H. Shi, L. Ao, W. Wang, Au/Cu₂O Schottky contact heterostructures with enhanced photocatalytic activity in dye decomposition and photoelectrochemical water splitting under visible light irradiation, *J. Alloys. Compd.* 684 (2016) 445–452, <https://doi.org/10.1016/j.jallcom.2016.05.192>.
- Y. Pan, S. Deng, L. Polavarapu, N. Gao, P. Yuan, C.H. Sow, Q.-H. Xu, Plasmon-enhanced photocatalytic properties of Cu₂O nanowire–Au nanoparticle assemblies, *Langmuir* 28 (2012) 12304–12310, <https://doi.org/10.1021/la301813v>.
- C.L. Bracey, P.R. Ellis, G.J. Hutchings, Application of copper-gold alloys in catalysis: current status and future perspectives, *Chem. Soc. Rev.* 38 (2009) 2231–2243, <https://doi.org/10.1039/b817729p>.
- C. Della Pina, E. Falletta, M. Rossi, Highly selective oxidation of benzyl alcohol to benzaldehyde catalyzed by bimetallic gold–copper catalyst, *J. Catal.* 260 (2008) 384–388, <https://doi.org/10.1016/j.jcat.2008.10.003>.
- W. Li, A. Wang, X. Liu, T. Zhang, Silica-supported Au–Cu alloy nanoparticles as an efficient catalyst for selective oxidation of alcohols, *Appl. Catal. A Gen.* 433–434 (2012) 146–151, <https://doi.org/10.1016/j.apcata.2012.05.014>.
- T. Tian, Y. Liu, X. Zhang, Bimetallic synergistic Au/Cu₂O-hydroxyapatite catalyst for aerobic oxidation of alcohols, *Chinese J. Catal.* 36 (2015) 1358–1364, [https://doi.org/10.1016/S1872-2067\(15\)60854-3](https://doi.org/10.1016/S1872-2067(15)60854-3).
- I. Nowak, M. Ziolek, Niobium compounds: preparation, characterization, and application in heterogeneous catalysis, *Chem. Rev.* 99 (1999) 3603–3624.
- M. Ziolek, I. Sobczak, The role of niobium component in heterogeneous catalysts, *Catal. Today* 285 (2017) 211–225, <https://doi.org/10.1016/j.cattod.2016.12.013>.
- K. Tanabe, Catalytic application of niobium compounds, *Catal. Today* 78 (2003) 65–77, [https://doi.org/10.1016/S0920-5861\(02\)00343-7](https://doi.org/10.1016/S0920-5861(02)00343-7).
- K. Ftouni, L. Lakiss, S. Thomas, M. Daturi, C. Fernandez, P. Bazin, J. El Fallah, M. El-Roz, J. El Fallah, M. El-Roz, TiO₂/zeolite bifunctional (photo)catalysts for a selective conversion of methanol to dimethoxymethane: on the role of Brønsted acidity, *J. Phys. Chem. C* 122 (2018) 29359–29367, <https://doi.org/10.1021/acs.jpcc.8b10092>.
- T. Murayama, W. Ueda, M. Haruta, Deposition of gold nanoparticles on niobium pentoxide with different crystal structures for room-temperature carbon monoxide oxidation, *ChemCatChem* 8 (2016) 1–6, <https://doi.org/10.1002/cctc.201600563>.
- S. Wuttke, P. Bazin, A. Vimont, C. Serre, Y.K. Seo, Y.K. Hwang, J.S. Chang, G. Férey, M. Daturi, Discovering the active sites for C3 separation in MIL-100(Fe) by using operando IR spectroscopy, *Chem. - A Eur. J.* 18 (2012) 11959–11967, <https://doi.org/10.1002/chem.201201006>.
- M. Thommes, K. Kaneko, A.V. Neimark, J.P. Olivier, F. Rodriguez-Reinoso, J. Rouquerol, K.S.W. Sing, Physisorption of gases, with special reference to the evaluation of surface area and pore size distribution (IUPAC Technical Report), *Pure Appl. Chem.* 87 (2015) 1051–1069, <https://doi.org/10.1515/pac-2014-1117>.
- T. Murayama, M. Haruta, Preparation of gold nanoparticles supported on Nb₂O₅ by deposition precipitation and deposition reduction methods and their catalytic activity for CO oxidation, *Chinese J. Catal.* 37 (2016) 1694–1701, [https://doi.org/10.1016/S1872-2067\(16\)62508-1](https://doi.org/10.1016/S1872-2067(16)62508-1).
- T. Murayama, J. Chen, J. Hirata, K. Matsumoto, W. Ueda, Hydrothermal synthesis of octahedra-based layered niobium oxide and its catalytic activity as a solid acid, *Catal. Sci. Technol.* 4 (2014) 4250–4257, <https://doi.org/10.1039/C4CY00713A>.
- J.H. Zhang, T. Zhu, N. Li, C.W. Xu, Glycerol electrooxidation on Au supported on carbon spheres by Stober method in alkaline medium, *Int. J. Electrochem. Sci.* 8 (2013) 9508–9517.
- K. Nakajima, J. Hirata, M. Kim, N.K. Gupta, T. Murayama, A. Yoshida, N. Hiyoshi, A. Fukuoka, W. Ueda, Facile formation of lactic acid from a triose sugar in water over niobium oxide with a deformed orthorhombic phase, *ACS Catal.* 8 (2018) 283–290, <https://doi.org/10.1021/acscatal.7b03003>.
- C. Yan, M.J. Wagner, Air- and water-stable gold-coated gadolinium metal nanocrystals, *Nano Lett.* 13 (2013) 2611–2614, <https://doi.org/10.1021/nl400720n>.
- X. Xie, J. Long, J. Xu, L. Chen, Y. Wang, Z. Zhang, X. Wang, Nitrogen-doped graphene stabilized gold nanoparticles for aerobic selective oxidation of benzylic alcohols, *RSC Adv.* 2 (2012) 12438–12446, <https://doi.org/10.1039/c2ra21291a>.
- H. Liu, N. Gao, M. Liao, X. Fang, Hexagonal-like Nb₂O₅ nanoplates-based photodetectors and photocatalyst with high performances, *Sci. Rep.* 5 (2015) 1–9, <https://doi.org/10.1038/srep07716>.
- C.L. Lin, S.L. Qiu, J. Chen, J.M. Tranquada, M. Strongin, The identification of oxygen related species in the XPS and near edge spectra of the high T_c superconductors, *Phys. C* 164 (1989) 1325–1326.
- V.I. Bukhtiyarov, M. Havecker, V.V. Kaichev, A. Knop-Gericke, R.W. Mayer, R. Schlögl, Atomic oxygen species on silver: photoelectron spectroscopy and X-ray absorption studies, *Phys. Rev. B* 67 (2003) 235422, <https://doi.org/10.1103/PhysRevB.67.235422>.
- V.V. Kaichev, V.I. Bukhtiyarov, M. Havecker, A. Knop-Gericke, R.W. Mayer, R. Schlögl, The nature of electrophilic and nucleophilic oxygen adsorbed on silver, *React. Kinet. Catal. Lett.* 44 (2003) 432–440, <https://doi.org/10.1023/A:1024459305551>.
- D.A. Svintitskiy, A.I. Stadnichenko, D.V. Demidov, S.V. Koscheev, A.I. Boromin, Investigation of oxygen states and reactivities on a nanostructured cupric oxide surface, *Appl. Surf. Sci.* 257 (2011) 8542–8549, <https://doi.org/10.1016/j.apsusc.2011.05.012>.
- L. Martin, H. Martinez, D. Poinot, B. Pecquenard, F. Le Cras, Direct observation of important morphology and composition changes at the surface of the CuO conversion material in lithium batteries, *J. Power Sources* 248 (2014) 861–873, <https://doi.org/10.1016/j.jpowsour.2013.10.015>.
- D.P. Dubal, G.S. Gund, R. Holze, H.S. Jadhav, C.D. Lokhande, C.J. Park, Surfactant-assisted morphological tuning of hierarchical CuO thin films for electrochemical supercapacitors, *Dalton Trans.* 42 (2013) 6459–6467, <https://doi.org/10.1039/C6CY01449F>.

c3dt50275a.

[43] Y. Wang, Y. Lü, W. Zhan, Z. Xie, Q. Kuang, L. Zheng, Synthesis of porous Cu₂O/CuO cages using Cu-based metal-organic frameworks as templates and their gas-sensing properties, *J. Mater. Chem. A Mater. Energy Sustain.* 3 (2015) 12796–12803, <https://doi.org/10.1039/C5TA01108F>.

[44] M.V. Kuznetsov, A.S. Razinkin, E.V. Shalaeva, Photoelectron spectroscopy and diffraction of surface nanoscale NbO/Nb(110) structures, *J. Struct. Chem.* 50 (2009) 514–521, <https://doi.org/10.1007/s10947-009-0079-y>.

[45] A. Gupta, M. Mittal, M.K. Singh, S.L. Suib, O.P. Pandey, Low temperature synthesis of Nb/C nano-composites as visible light photoactive catalyst, *Sci. Rep.* 8 (2018) 13597, <https://doi.org/10.1038/s41598-018-31989-z>.

[46] J. Socratos, K.K. Banger, Y. Vaynzof, A. Sadhanala, A.D. Brown, A. Sepe, U. Steiner, H. Sirringhaus, Electronic structure of low-temperature solution-processed amorphous metal oxide semiconductors for thin-film transistor applications, *Adv. Funct. Mater.* 25 (2015) 1873–1885, <https://doi.org/10.1002/adfm.201404375>.

[47] T.V. Larina, L.S. Dovlitova, V.V. Kaichev, V.V. Malakhov, T.S. Glazneva, E.A. Paukshits, B.S. Bal'Zhinimaev, Influence of the surface layer of hydrated silicon on the stabilization of Co²⁺ cations in Zr-Si fiberglass materials according to XPS, UV-Vis DRS, and differential dissolution phase analysis, *RSC Adv.* 5 (2015) 79898–79905, <https://doi.org/10.1039/c5ra12551k>.

[48] B. Grzyb, S. Gryglewicz, A. Śliwak, N. Díez, J. Machnikowski, G. Gryglewicz, Guanidine, amitrole and imidazole as nitrogen dopants for the synthesis of N-graphenes, *RSC Adv.* 6 (2016) 15782–15787, <https://doi.org/10.1039/C5RA24624E>.

[49] V.S. Braga, J.A. Dias, S.C.L. Dias, J.L. De Macedo, Catalyst materials based on Nb₂O₅ supported on SiO₂–Al₂O₃: preparation and structural characterization, *Chem. Mater.* 17 (2005) 690–695, <https://doi.org/10.1012/cm048673u>.

[50] L.J. Burcham, J. Datka, I.E. Wachs, In situ vibrational spectroscopy studies of supported niobium oxide catalysts, *J. Phys. Chem. B* 103 (1999) 6015–6024, <https://doi.org/10.1021/jp990289a>.

[51] M. Compagnoni, S.A. Kondrat, C.E. Chan-Thaw, D.J. Morgan, D. Wang, L. Prati, A. Villa, N. Dimitratos, I. Rossetti, Spectroscopic investigation of titania-supported gold nanoparticles prepared by a modified deposition/precipitation method for the oxidation of CO, *ChemCatChem.* 8 (2016) 2136–2145, <https://doi.org/10.1002/cctc.201600072>.

[52] G. Mamba, C. Pulgarin, J. Kiwi, M. Bensimon, S. Rtimi, Synchronic coupling of Cu₂O(p)/CuO(n) semiconductors leading to Norfloxacin degradation under visible light: kinetics, mechanism and film surface properties, *J. Catal.* 353 (2017) 133–140, <https://doi.org/10.1016/j.jcat.2017.06.036>.

[53] X. Liu, A. Wang, L. Li, T. Zhang, C.Y. Mou, J.F. Lee, Structural changes of Au-Cu bimetallic catalysts in CO oxidation: in situ XRD, EPR, XANES, and FT-IR characterizations, *J. Catal.* 278 (2011) 288–296, <https://doi.org/10.1016/j.jcat.2010.12.016>.

[54] A. Wang, X.Y. Liu, C.Y. Mou, T. Zhang, Understanding the synergistic effects of gold bimetallic catalysts, *J. Catal.* 308 (2013) 258–271, <https://doi.org/10.1016/j.jcat.2013.08.023>.

[55] C. Huo, J. Ouyang, H. Yang, CuO nanoparticles encapsulated inside Al-MCM-41 mesoporous materials via direct synthetic route, *Sci. Rep.* 4 (2015) 3682, <https://doi.org/10.1038/srep03682>.

[56] Y. Zhou, Z. Qiu, M. Lü, A. Zhang, Q. Ma, Preparation and spectroscopic properties of Nb₂O₅ nanorods, *J. Lumin.* 128 (2008) 1369–1372, <https://doi.org/10.1016/j.jlumin.2008.01.001>.

[57] G. Corro, S. Cebada, U. Pal, J.L.G. Pierro, Au⁰-Au³⁺ bifunctional site mediated enhanced catalytic activity of Au/ZnO composite in diesel particulate matter oxidation, *J. Catal.* 347 (2017) 148–156, <https://doi.org/10.1016/j.jcat.2017.01.011>.

[58] X. Zou, H. Fan, Y. Tian, S. Yan, Synthesis of Cu₂O/ZnO hetero-nanorod arrays with enhanced visible-light-driven photocatalytic activity, *CrystEngComm.* 16 (2014) 1149–1156, <https://doi.org/10.1039/C3CE42144A>.

[59] X. Jiang, Q. Lin, M. Zhang, G. He, Z. Sun, Microstructure, optical properties, and catalytic performance of Cu₂O-modified ZnO nanorods prepared by electrodeposition, *Nanoscale Res. Lett.* 10 (2015) 2–7, <https://doi.org/10.1186/s11671-015-0755-0>.

[60] D. Baojuan, L. Shumin, L. Deliang, Z. Ruozhu, L. Jingge, H. Qinglan, B. Feng, Catalytic oxidation of ethyl acetate and toluene over Cu-Ce-Zr supported ZSM-5/TiO₂ catalysts, *RSC Adv.* 6 (2016) 53852–53859, <https://doi.org/10.1039/c6ra06421c>.

[61] Y. Gotoh, R. Igarashi, Y. Ohkoshi, M. Nagura, K. Akamatsu, S. Deki, Preparation and structure of copper nanoparticle/poly(acrylic acid) composite films, *J. Mater. Chem.* 10 (2000) 2548–2552, <https://doi.org/10.1039/b003899g>.

[62] L. Liu, Z. Yao, B. Liu, L. Dong, Correlation of structural characteristics with catalytic performance of CuO/Ce_xZr_{1-x}O₂ catalysts for NO reduction by CO, *J. Catal.* 275 (2010) 45–60, <https://doi.org/10.1016/j.jcat.2010.07.024>.

[63] B. Choudhury, M. Dey, A. Choudhury, Shallow and deep trap emission and luminescence quenching of TiO₂ nanoparticles on Cu doping, *Appl. Nanosci.* 4 (2014) 499–506, <https://doi.org/10.1007/s13204-013-0226-9>.

[64] F.A.C. Garcia, V.S. Braga, J.C.M. Silva, J.A. Dias, S.C.L. Dias, J.L.B. Davo, Acidic characterization of copper oxide and niobium pentoxide supported on silica-alumina, *Catal. Letters* 119 (2007) 101–107, <https://doi.org/10.1007/s10562-007-9204-8>.

[65] F. Hemmann, C. Jaeger, E. Kemnitz, Comparison of acidic site quantification methods for a series of nanoscopic aluminum hydroxide fluorides, *RSC Adv.* 4 (2014) 56900–56909, <https://doi.org/10.1039/c4ra09477h>.

[66] J. Datka, A.M. Turek, J.M. Jehng, I.E. Wachs, Acidic properties of supported niobium oxide catalysts: an infrared spectroscopy investigation, *J. Catal.* 135 (1992) 186–199, [https://doi.org/10.1016/0021-9517\(92\)90279-Q](https://doi.org/10.1016/0021-9517(92)90279-Q).

[67] K. Nakajima, Y. Baba, R. Noma, M. Kitano, J.N. Kondo, S. Hayashi, M. Hara, Nb₂O₅·nH₂O as a heterogeneous catalyst with water-tolerant lewis acid sites, *J. Am. Chem. Soc.* 133 (2011) 4224–4227, <https://doi.org/10.1021/ja110482r>.

[68] J. Lee, H.S. Shim, M. Lee, J.K. Song, D. Lee, Size-controlled electron transfer and photocatalytic activity of ZnO-Au nanoparticle composites, *J. Phys. Chem. Lett.* 2 (2011) 2840–2845, <https://doi.org/10.1021/jz2013352>.

[69] P. She, K. Xu, Q. He, S. Zeng, H. Sun, Z. Liu, Controlled preparation and visible light photocatalytic activities of corn cob-like Au-ZnO nanorods, *J. Mater. Sci.* 52 (2017) 3478–3489, <https://doi.org/10.1007/s10853-016-0639-4>.

[70] S.N. Haberreuter, L. Schmidt-Mende, J.K. Stolarczyk, Photocatalytic reduction of CO₂ on TiO₂ and other semiconductors, *Angew. Chemie - Int. Ed.* 52 (2013) 7372–7408, <https://doi.org/10.1002/anie.201207199>.

[71] L. Xiao, T. Su, Z. Wang, K. Zhang, X. Peng, Y. Han, Q. Li, X. Wang, Enhanced photocatalytic hydrogen evolution by loading Cd_{0.5}Zn_{0.5}S QDs onto Ni₂P porous nanosheets, *Nanoscale Res. Lett.* 13 (2018) 1–9, <https://doi.org/10.1186/s11671-018-2438-0>.

[72] N. Wu, Plasmonic metal-semiconductor photocatalysts and photoelectrochemical cells: a review, *Nanoscale.* 10 (2018) 2679–2696, <https://doi.org/10.1039/cnr08487k>.

[73] J. Li, S.K. Cushing, J. Bright, F. Meng, T.R. Senty, P. Zheng, A.D. Bristow, N. Wu, Ag@Cu₂O core-shell nanoparticles as visible-light plasmonic photocatalysts, *ACS Catal.* 3 (2013) 47–51, <https://doi.org/10.1021/cs300672f>.

[74] V.V. Kaichev, G.Y. Popova, Y.A. Chesarov, A.A. Saraev, D.Y. Zemlyanov, S.A. Beloshapkin, A. Knop-Gericke, R. Schlögl, T.V. Andrushkevich, V.I. Bukhityarov, Selective oxidation of methanol to form dimethoxymethane and methyl formate over a monolayer V₂O₅/TiO₂ catalyst, *J. Catal.* 311 (2014) 59–70, <https://doi.org/10.1016/j.jcat.2013.10.026>.

[75] C.-C. Chuang, W.-C. Wu, M.-C. Huang, J.-L. Lin, FTIR study of adsorption and reactions of methyl formate on powdered TiO₂, *J. Catal.* 185 (1999) 423–434, <https://doi.org/10.1006/jcat.1999.2516>.

[76] K.A. Thavorprasert, M. Capron, L. Jalowiecki-Duhamel, F. Dumeignil, One-pot 1,1-dimethoxymethane synthesis from methanol: a promising pathway over bifunctional catalysts, *Catal. Sci. Technol.* 6 (2016) 958–970, <https://doi.org/10.1039/c5cy01858g>.

[77] S. Chen, X. Ma, The role of oxygen species in the selective oxidation of methanol to dimethoxymethane over VO_x/TS-1 catalyst, *J. Ind. Eng. Chem.* 45 (2017) 296–300, <https://doi.org/10.1016/j.jiec.2016.09.037>.

[78] N. Li, S. Wang, Y. Sun, S. Li, First principles studies on the selectivity of dimethoxymethane and methyl formate in methanol oxidation over V₂O₅/TiO₂-based catalysts, *Phys. Chem. Chem. Phys.* 19 (2017) 19393–19406, <https://doi.org/10.1039/c7cp02326j>.

[79] G. Busca, A. Elmí, P. Forzatti, Mechanism of selective methanol oxidation over vanadium oxide-titanium oxide catalysts: a FT-IR and flow reactor study, *J. Phys. Chem.* 91 (1987) 5263–5269, <https://doi.org/10.1021/j100304a026>.

[80] J. Low, C. Jiang, B. Cheng, S. Wageh, A.A. Al-Ghamdi, J. Yu, A review of direct Z-scheme photocatalysts, *Small Methods* 1 (2017) 1700080, <https://doi.org/10.1002/smtd.201700080>.

[81] J. Fu, S. Cao, J. Yu, Dual Z-scheme charge transfer in TiO₂–Ag–Cu₂O composite for enhanced photocatalytic hydrogen generation, *J. Mater. 1* (2015) 124–133, <https://doi.org/10.1016/j.jmat.2015.02.002>.

[82] M.L. Personick, R.J. Madix, C.M. Friend, Selective oxygen-assisted reactions of alcohols and amines catalyzed by metallic gold: paradigms for the design of catalytic processes, *ACS Catal.* 7 (2017) 965–985, <https://doi.org/10.1021/acscatal.6b02693>.

[83] L. Sinatra, A.P. Lagrow, W. Peng, A.R. Kirmani, A. Amassian, H. Idriss, O.M. Bakr, A Au/Cu₂O-TiO₂ system for photo-catalytic hydrogen production. A pn-junction effect or a simple case of in situ reduction? *J. Catal.* 322 (2015) 109–117, <https://doi.org/10.1016/j.jcat.2014.11.012>.

[84] A. Kormányos, A. Thomas, M.N. Huda, P. Sarker, J.P. Liu, N. Poudyal, C. Janáky, K. Rajeshwar, Solution combustion synthesis, characterization, and photoelectrochemistry of CuNb₂O₆ and ZnNb₂O₆ nanoparticles, *J. Phys. Chem. C* 120 (2016) 16024–16034, <https://doi.org/10.1021/acs.jpcc.5b12738>.